THE JOURNAL OF PHYSICAL CHEMISTRY C

Article

pubs.acs.org/JPCC

Adsorption and Diffusion of Hydrogen on the Surface of the Pt_{24} Subnanoparticle. A DFT Study

Stanislav K. Ignatov,*[,†] Andrey I. Okhapkin,[†,‡] Oleg B. Gadzhiev,[†] Alexey G. Razuvaev,[†,‡] Sebastian Kunz,[§] and Marcus Bäumer[§]

[†]N.I. Lobachevsky State University of Nizhny Novgorod, Nizhny Novgorod, Russia

[‡]Research Institute of Chemistry of University of Nizhny Novgorod, Nizhny Novgorod, Russia

[§]University of Bremen, Bremen, Germany

Supporting Information

ABSTRACT: Platinum and platinum based materials are of fundamental importance for modern and developed catalysts, fuel cells, sensors, hydrogen production and storage systems, and nanoelectronic devices. The subnanosize cluster Pt_{24} was considered as a model of the prospective catalytic system based on the oxide and carbide supported Pt nanoparticles (Pt NPs) or Pt NPs with soft spacers anchored to their surface. Structural, electronic, thermodynamic, and spectral properties of the adsorption complexes of molecular and atomic hydrogen on Pt NPs have been studied using the DFT method (the BLYP functional with the 6-31G(p) basis for H and the CRENBS pseudopotential for Pt atoms). On this basis, the adsorption energies for molecular hydrogen at the Pt NPs along with the energies and activation energies of its dissociation were estimated and the pathways of activationless dissociative adsorption were found. The full map of adsorption energies of atomic hydrogen at the various surface regions of Pt_{24} was obtained. The structures of transition states for the rearrangements between the adsorption complexes were located, and the activation energies for surface migration were calculated. Additionally, several ways of subsurface diffusion of H atoms inside the Pt_{24} cluster were considered which allows estimating the diffusion parameters and the probability of the hydrogen spillover when the cluster surface is highly covered by ligands restricting the surface migration. The IR and Raman spectra of most favorable adsorption complexes were simulated to provide the possibility of an experimental validation of the results obtained.

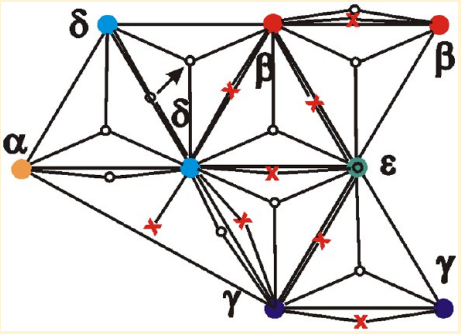

INTRODUCTION

The interaction of molecular and atomic hydrogen with metal surfaces is one of the most fundamental processes lying in a ground of many modern and probably future technologies. One of such technologies is the alternative and sustainable energy sector where hydrogen is a prospective environment-friendly and highly efficient fuel.[1−3] A complementary line to these ground breaking technologies is the development of H_2 sensors and other control devices where the hydrogen interaction with the solid surface is the main process forming the analytical signal.[4−6] For electrochemistry, hydrogen adsorption represents processes of fundamental importance involved in the Tafel and Volmer reactions of electrochemical oxidation.[7,8] Another important field for the hydrogen/metal interaction studies is the catalysis in the fine chemical synthesis for the food, pharmaceutical, cosmetological, and fragrance industries. For example, in the fragrance technology, the selective hydrogenation of unsaturated aldehydes occurring with the new composite catalysts based on the oxide supported platinum nanoparticles (Pt NPs) with the chemically modified surface is of special interest. The discovery of such a kind of processes in the end of the 1990s opened new ways in the development of highly effective catalysts which can provide high regio-, chemo-, and, probably, stereoselectivity.[9−14] It is worthwhile to mention another modern direction of Pt NP applications—the development of prospective spintronic and quantum devices (i.e., memory devices and quantum bits) based on the small size-selected metal clusters.[15,16] For such applications, the electronic and spin properties of the subnanosized particles (probably staying in contact with the gas phase) are of particular interest.[17]

The studies of hydrogen interaction with the platinum surface, both experimental and theoretical, have a long history[18−25] (for the detailed historical assay, see the monograph[26] and references therein). The experimental adsorption energy of H_2 on the Pt(111) surface was obtained[18] using LEED, ELS, TDS, and contact potential experiments. Two adsorption states were found corresponding to the low and higher coverage with maximum activation energy of desorption of 9.5 kcal/mol. The adsorption energy for sub-ML coverages of H atoms on Pt(111) was measured in the study[19] using the He beam diffraction technique. The obtained value

Received: May 5, 2016
Revised: July 18, 2016
Published: July 27, 2016

DOI: 10.1021/acs.jpcc.6b04555
J. Phys. Chem. C 2016, 120, 18570−18587

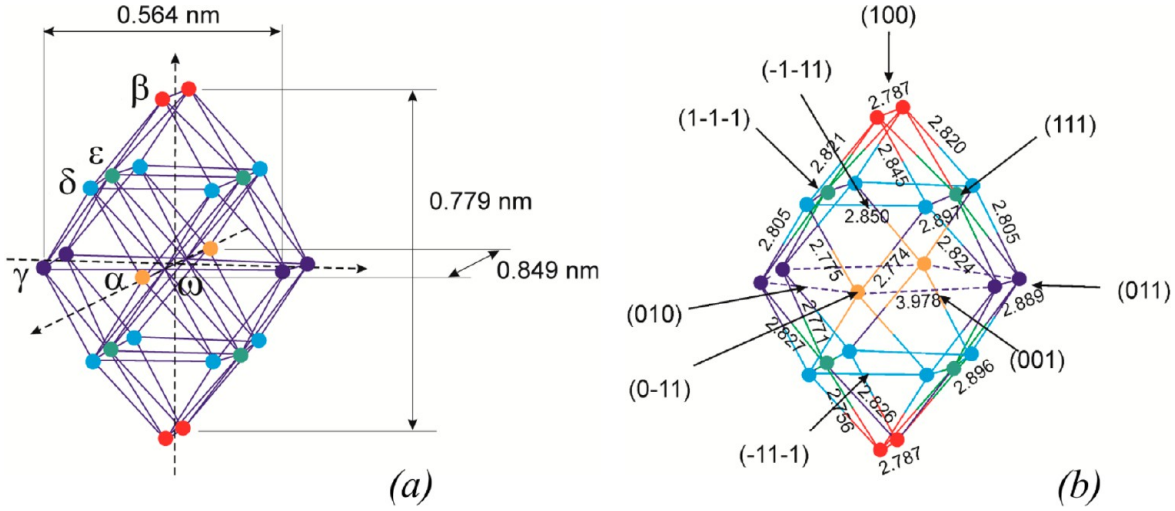

Figure 1. Optimized structure of the Pt_{24} cluster (M = 5, distorted D_{2h} symmetry group): (a) designation of the atom types; (b) selected surface bond lengths (Å) and the normal directions for the corresponding microfacet planes.

was 8.6 kcal/mol relative to the free H_2 molecule. Graham et al.[22] estimated the activation energy of the H and D surface diffusion on Pt(111) using the quasielastic helium atom scattering measurements as 68 meV (1.6 kcal/mol relative to H_2). This value is remarkably different from the results obtained in linear optical direction (LOD) experiments by Zheng et al.[27] where fitted data for the thermally activated diffusion are given as 4.3 and 4.4 kcal/mol for flat and stepped surfaces of Pt(111), respectively. Badescu et al.[24] estimated the effect of vibrational excitations of adsorbed H atoms on the basis of HREELS spectra and compared it to the calculated vibrational bands of the adsorbed H atoms. It was concluded that the surface migration of H atoms on the Pt surface is remarkably influenced by the effect of quantum tunneling. The hydrogen adsorption of Pt(100) was studied in refs 20 and 21. Using the LEED, TDS, and work function measurements, however, the direct estimation of the adsorption energy was unavailable. Recently, the authors of ref 25 carried out the combined experimental and theoretical study of the hydrogen TPD spectra on the reconstructed Pt(110) surface. Using the periodic calculations (the RPBE functional over the plane wave basis), the H atom adsorption energy on the reconstructed (110) face ridge was estimated in the range from 6.5 to 9.2 kcal/mol (depending on the coverage) per single H atom and as 5.3 kcal/mol for the FCC site of the (111) microfacet.

The detailed information on the state of hydrogen on the metal surface as well as on the surface of NPs of platinum and its alloys can be obtained by theoretical studies. Among them, some recent quantum chemical studies of structures and energies of adsorption complexes of hydrogen can be mentioned[28−36] as well as the combined experimental and theoretical studies.[24,25] To date, the energy of adsorption and mechanisms of the H atom migration and desorption on ideal and stepped surfaces were estimated in the studies[28−31,34,36] along with the activation energies for desorption, surface migration, and subsurface diffusion.[24,32,33] The adsorption energies of H_2 onto platinum surfaces (100) and (111) in different coordination modes, i.e., top, bridge, and both hollow sites (HCP and FCC), calculated for different coverages mainly with the slab model were summarized by Zyubin et al.[37] where also adsorption on the (110) surface was studied as well as activation energies for H atom migration. Many theoretical studies are devoted to the structure and properties of the Pt clusters and nanoparticles of a broad range of sizes from several atoms to tens and hundreds of atoms[28,29,38−43] as well as the hydrogen interaction with them.[28,30,44−47] Recently, the study of the Pt and Pd NPs deposited at the MgO support was performed.[48,49] The authors considered the H_2 adsorption on the Pt_{127} periodic clusters with the FCC structure and found several coordination modes for the H atoms with the adsorption energies in a range of 3.9−8.8 kcal/mol. It should be noted that the sizes of NPs larger than 1.6 nm in size considered in refs 48 and 49 are mostly applicable to the "classical" nanocatalysts. The NPs of smaller size are more relevant to the NP's deposited in the zeolite pores[50] and to the size-selected clusters generated by the modern experimental techniques[15,16] (such clusters are especially important for the magnetochemical and spintronic applications[17]).

It should be noted that most theoretical studies were carried out with periodic calculations which present NPs as a part of infinite periodic layers. Such a representation has significant computational advances because the DFT calculations over the plane wave basis are very efficient with highly scalable algorithms implemented in quantum chemical programs and allow calculating rather large clusters or slab regions. However, at the same time, this potentially leads to an incorrect description of local structures and inhomogeneities. First, the high coverage of the surface for bulky catalyst results in the fictitious interaction of an atom with its "ghost" generated by periodic boundary conditions. This can result in the fictitious stabilization of the surface structures with high dipole moments. Second, one of the very effective and, as a consequence, frequently used approaches of the periodic modeling is spin-unpolarized calculations which can lead to a loss of information on the manifold of spin multiplicities. Thus, the fundamental quantum property is not covered in these calculations. Due to this, for example, the probable spin recoupling in hydrogen activation is not correctly treated. This also makes the development and modeling of quantum and spintronic devices within this approximation impossible. In contrast, with a periodic approach, we are concentrated on another theoretical model which is probably more suitable for the broad range of tasks for the modeling of the various future nanosystems including the supported composite catalysts, gas sensors, and

DOI: 10.1021/acs.jpcc.6b04555
J. Phys. Chem. C 2016, 120, 18570−18587

the nanosystems with interacting NPs where reactions occur between the faces of different NPs. For such tasks, the medium-size clusters should be considered providing the way to model several interacting NPs. Then, we should consider the unordered NP surfaces in different spin states without restrictions imposed due to periodic approximation.

In the presented study, we carried out the DFT calculations of the hydrogen interactions with the platinum nanoparticle using a finite cluster model. We try to describe the processes of the hydrogenation of Pt NPs occurring with modern catalysts containing the SiO_2 or TiO_2 supported Pt NPs which were recently synthesized experimentally.[51] The minimum size of the synthesized NPs was about 1.2 nm which corresponds to the cluster containing approximately 100 atoms. Conventional Pt nanoparticle deposition techniques based on wet chemistry methods result in a relatively wide and multimaximum particle size and shape distribution, while an atomic layer deposition (ALD) represents a prospective and alternative way to low-loads (nano)catalysts design with a very fine control of particle size distribution (high probability of fabrication of 1 nm particles and averaged diameter of 1.5 ± 0.35 Å).[50] The conditions, including Pt low-loading, where 1−5 nm distribution with a maximum in the range 1−2 nm, are often employed conditions for standard industrial catalyst prepared commercially,[52−54] e.g., EUROPT-1, Pt/Vulcan XC 72 by E-TEK or Degussa AG, or developed[50] zeolite and silicon (Y, SBA-15 etc.) based catalysts (see also refs 15 and 16 and references therein). Thus, to provide a quantitative description of such NPs, we need the cluster of the similar size possessing the structural features of the real NPs. Because the real distribution of the face types on the surface of NPs is unknown and, probably, changes during the catalyst life-cycle, it is reasonable to choose the cluster having a set of different faces.

A useful model for a supported Pt NP catalyst is a cluster Pt_{24} (see Figure 1a). This cluster is a subnanosized structure with a size of 0.849 × 0.779 × 0.564 nm^3. We did not use the symmetry restraints in our calculations; thus, the exact point groups of the cluster is C_1. However, the cluster structure is rather symmetric and only slightly different from the D_{2h} group in all of the spin states we considered (see below). For example, the differences in the bond lengths between the atoms which are equivalent in the structure of D_{2h} symmetry are typically not more than 0.01 Å. The important feature of the Pt_{24} cluster is that its surface corresponds to the several different crystallographic faces with low indices, including (111), (100), (001), and (011) (see Figure 1b). Thus, we can explore the adsorption on different faces and sites as well as the surface migration of adsorbed species between different faces within the same cluster. At the same time, some regions of the same faces (e.g., (111)) are rather broad, which allows exploring the surface diffusion as well as the adsorption and reactions of multiple hydrogen molecules or atoms on the same face within the single cluster.

The main objective of the present study is exploring the electronic, spin, and thermodynamic properties of the Pt_{24} subnanoparticle along with the characteristic structures of adsorption complexes formed by molecular and atomic hydrogen at the surface of Pt NPs. For these complexes, we estimate their energies and thermodynamic parameters in order to find the most favorable structures formed at the surface as well as the activation energies for the surface dissociation of molecular hydrogen and the activation energies for the surface migration of formed hydrogen atoms. Additionally, we estimate the diffusion ability of hydrogen atoms inside the Pt NPs in terms of activation energies of their diffusion inside the Pt cluster. The last question is closely connected to the question on the possibility of the spillover process occurring via internal diffusion of hydrogen from the upper region of the surface to the oxide support at the opposite NP surface. This process can be efficient in the case of the surface highly covered by the ligands hindering the surface migration. Finally, we model the IR and Raman spectra of the adsorption hydrogen complexes which can, in principle, provide a way of experimental registration of the modeled structures and a method for the validation of theoretical results obtained here.

■ COMPUTATIONAL METHODS

All of the calculations were carried out with the DFT method using the BLYP functional. The 6-31G(p) basis set was used for the H atoms. The *ab initio* relativistic effective core pseudopotential with spin−orbit operator (CRENBS)[55] in conjunction with the corresponding basis set was utilized for Pt atoms. The Gaussian 03 program[56] was used for all of the calculations. The spin-unrestricted formulation of the DFT theory (UBLYP) was used for all of the structures with unpaired spins. The full geometry optimizations were performed for all of the coordinated structures. All of the located stationary PES points were characterized by the frequency calculations. Original programs were used for the structure construction and selection. The MOLTRAN program[57,58] was applied for the input data preparation and thermodynamic calculations. The ChemCraft[59] software was used for visualization and graphical data preparation.

■ RESULTS

Structural Features of the Pt_{24} Cluster. If the symmetry group of the Pt_{24} cluster is considered as a slightly distorted D_{2h}, the cluster contains only six types of atoms which we designate with Greek letters as α, β, ε, δ, γ, and ω (see Figure 1a). Among them, only five atom types (α, β, ε, δ, γ) are the surface atoms, whereas two ω atoms belong to the subsurface layer. In order to make figures more informative, we will use different colors for the five surface atoms, as shown in Figure 1b. The surface of the Pt_{24} cluster contains nine bond types ($\beta\beta$, $\gamma\gamma$, $\delta\delta$, $\beta\delta$, $\beta\varepsilon$, $\gamma\delta$, $\gamma\varepsilon$, $\alpha\gamma$, $\alpha\delta$, $\delta\varepsilon$) and can be divided into only six unique types of triangular regions ($\beta\beta\varepsilon$, $\beta\delta\varepsilon$, $\beta\delta\delta$, $\gamma\gamma\varepsilon$, $\gamma\delta\varepsilon$, $\alpha\gamma\delta$, $\alpha\delta\delta$). Among the surface regions, there are two adjacent $\alpha\gamma\delta$ regions forming the square regions $\alpha\delta\gamma\delta$ without the diagonal chemical bonds. However, it is more convenient to describe the adsorption properties of this region considering two triangular parts. The volume structure of the Pt_{24} cluster has also only several unique polyhedrons, namely, four tetrahedrons ($\beta\beta\varepsilon\varepsilon$, $\beta\gamma\varepsilon\omega$, $\alpha\delta\delta\omega$, $\varepsilon\varepsilon\omega\omega$), and three square pyramids ($\beta\delta\delta\varepsilon\varepsilon$, $\gamma\gamma\varepsilon\omega\omega$, $\delta\delta\varepsilon\varepsilon\omega$). Among the last ones, two adjacent pyramids can also be considered as two octahedrons ($\beta\delta\delta\varepsilon\varepsilon\omega$, $\gamma\gamma\varepsilon\varepsilon\omega\omega$). Thus, from the computational point of view, the Pt_{24} cluster is a very convenient model due to the fact of the restricted number of unique structural features. Therefore, one can explore all the feasible adsorption modes on the cluster as well as all the feasible diffusion regimes inside the NP.

Energies of Spin States. The Pt_{24} cluster has 240 valence electrons (within the CRENBS pseudopotential) and can exist in different spin states of a relatively low energy. The optimized structures of the spin states corresponding to the odd

DOI: 10.1021/acs.jpcc.6b04555
J. Phys. Chem. C 2016, 120, 18570−18587

Table 1. Calculated Total Energies E_{tot} (Hartree), Spin Square Values before (S^2) and after (S^2_A) Annihilation, the Energies Relative to the Quintet (Ground) State ΔE (kcal/mol), and the Corresponding Enthalpies ΔH^0 (kcal/mol) and the Gibbs Free Energies ΔG^0 (kcal/mol) at Different Temperatures for the Different Spin States of the Pt_{24} Cluster

state mult.	E_{tot}	S^2	S^2_A	ΔE	ΔH^0(0 K)	ΔH^0(298 K)	ΔG^0(298 K)	ΔH^0(500 K)	ΔG^0(500 K)
1	−658.7711294	0	0	5.89	7.25	7.28	7.14	7.28	7.05
3	−658.8107444	3.78	4.24	0.61	0.65	0.62	1.73	0.62	2.48
5	−658.8117239	6.69	6.11	0.00	0.00	0.00	0.00	0.00	0.00
7	−658.8102780	12.23	12.00	0.91	0.82	0.31	1.80	−0.09	2.91
9	−658.8105520	20.04	20.00	0.74	0.57	0.71	−1.25	0.72	−2.58
11	−658.7908935	30.03	30.00	13.07	12.76	12.44	11.34	12.06	10.71
13	−658.7689607	42.03	42.00	26.83	26.63	26.81	25.16	26.81	24.05
15	−658.7427680	56.03	56.00	43.27	43.12	43.26	41.19	43.26	39.78

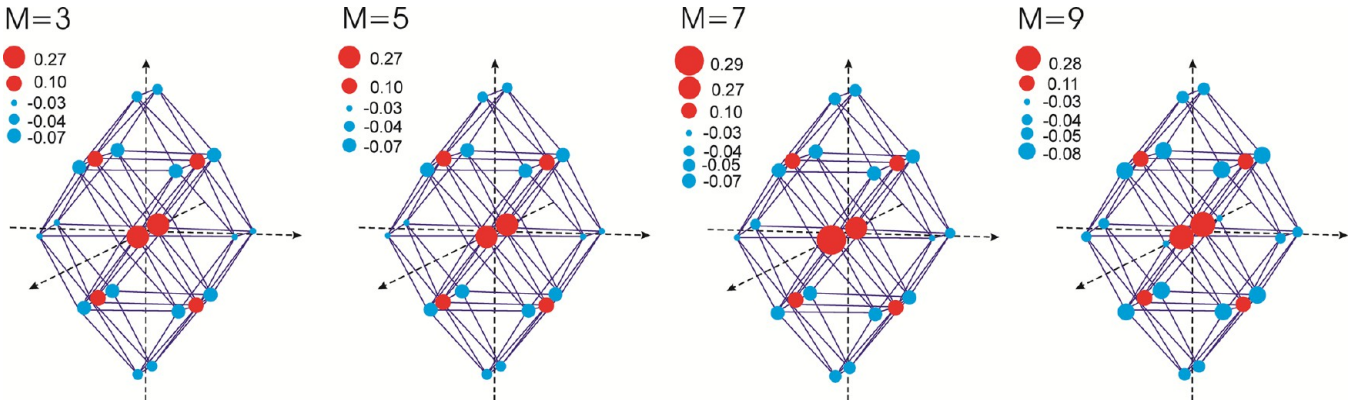

Figure 2. Calculated Mulliken charges Pt_{24} for different spin states.

multiplicities M from 1 to 15 are in general close to each other, and the symmetry of the cluster in all the considered spin states is only slightly different from the D_{2h} group. The energies of all the spin states are given in Table 1. As is evident from the table, the ground state of the cluster corresponds to the quintet spin state. However, there exists a group of spin states (M = 3, 5, 7, 9) with energies very close to the energy of the ground state (in a range of 1 kcal/mol). The energies of other spin states are significantly higher, at least by several kcal/mol and higher. Below, we will show that not only energies but also other properties of the low-lying spin states of Pt_{24} are rather close to each another and, thus, we can consider the only spin state (ground spin state, M = 5) as a most representable state for the description of the adsorption and diffusion properties of the NP.

The optimized ground state (M = 5) of the cluster structure shown in Figure 1 is more favorable in energy than the structure obtained in the DFT optimization (at the same level of theory) of the global minimum structure of Pt_{24} found earlier by Doye and Wales[60] with the Sutton−Chen empirical potential.[61] Later, the similar structure was located for the Pt_{24} using the Voter−Chen version of the EAM potential in the studies of Sebetci and Güvenç.[62,63] It is interesting that the optimized structures of Pt_{23} and Pt_{25} located by Nie et al.[64] at the DFT (PW91/DZP+ECP) level were the FCC-like and icosahedral-like ones rather distinct from the shape of Pt_{24} considered here. The global optimization of Pt_{24} using the Gupta potential[65] carried out by us with the ABCluster program[66] also leads to a structure similar to that located in ref 60. This fact takes place for the states of M = 3, 5, 7, 9 of the Doye−Wales structure, and the lowest energy of the DFT optimized Doye−Wales structures (M = 9) is about 1.3 kcal/mol higher than the ground state (M = 5) of the Pt_{24} structure considered here (Figure 1). Thus, although we did not perform the exhaustive global optimization of Pt_{24} at the DFT level, we believe that the structure found by us is one of the most (if not the very most) favorable in energy among the low-lying minima of the Pt_{24} cluster.

The spin states obtained at the UDFT level are mostly pure; the calculated S^2 values are only slightly different from the pure $S(S + 1)$ eigenvalues of the spin operator for all the spin states except the triplet one. In the case of the triplet system, however, we failed to locate the pure spin state even after the spin projection. After annihilation, the spin square is increased, which demonstrates the effect observed earlier on other molecular systems. This effect was discussed earlier by Davidson and Clark[67] and Plakhutin et al.[68] and is explained by the fact that the spin state is contaminated by the higher order spin admixtures which are more dominant after the annihilation of the first order spin component. This fact is a consequence of the restricted description of the spin state in the framework of the single-reference wave functions and has no solution up to date within the DFT theory, both for the cluster and periodic models. Although such effects do not result usually in the significant energy changes, this fact stresses that the description of the different spin states of the metal clusters is a subject of subtle effects which require the careful consideration in order to give the proper physical description.

Electronic Charges and Spin Densities. Four low-lying spin states of Pt_{24} (M = 3, 5, 7, 9) have quite similar Mulliken charge distributions (see Figure 2). The most positive Mulliken charges are located at two central (ω) atoms, whereas the atoms located at vertices are always negatively charged. The value of the negative charge at the vertex atoms is slightly different in the different spin states, but as a rule, the δ-atoms are more negative than the β and γ ones. The α-atoms are the

DOI: 10.1021/acs.jpcc.6b04555
J. Phys. Chem. C 2016, 120, 18570−18587

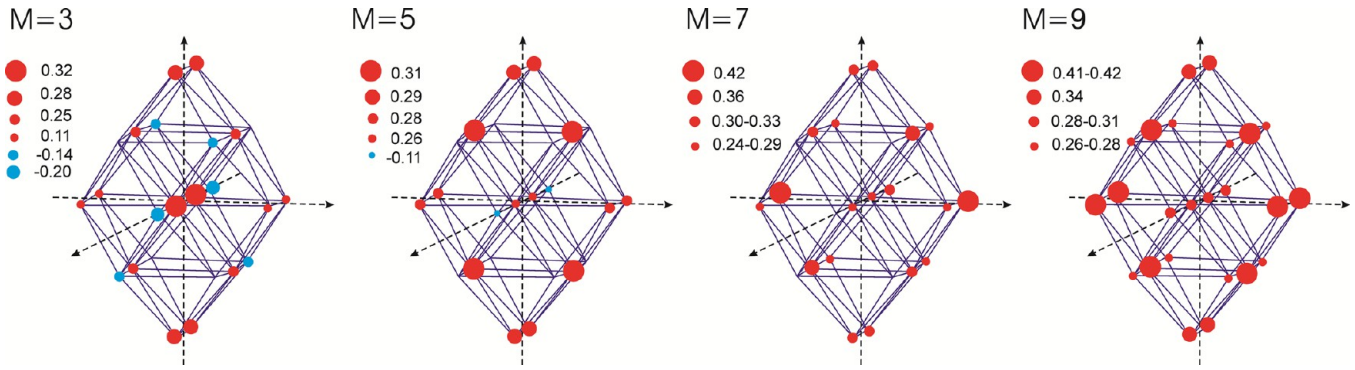

Figure 3. Calculated Mulliken spin densities of Pt_{24} for different spin states.

most electroneutral ones. The ε-atoms are always positively charged. Thus, all the optimized structures of low-lying spin states show the same sequence for the Mulliken charges:

$$q(\delta) < q(\beta) < q(\gamma) < q(\alpha) \leq 0 < q(\varepsilon) < q(\omega)$$

In all the low-lying spin states, the Mulliken charge distribution is described well by the fully symmetric irreducible representation of the idealized D_{2h} group. The only significant deviation takes place for the $M = 7$ state, where remarkable asymmetry is found between the γ and ω atom sets (see Figure 2).

In contrast with the Mulliken charges, the spin density distribution (Figure 3) is more spatially asymmetric due to the fact that the single occupied molecular orbitals are transformed by the not fully symmetric irreducible representations of the D_{2h} group. Again, the significant asymmetry takes place for the $M = 7$ state where the γ spin densities are essentially different. In the case of $M = 3$ and, especially, $M = 9$, the spin density distribution of Pt_{24} is very symmetric. In all of the considered spin states, the spin densities of the same atoms are remarkably different. In the ground state ($M = 5$), the atoms having the highest spin density are the ε ones, whereas the free spins reside at the γ atoms in the $M = 7$ and 9 states. For the triplet state, the highest spin density is concentrated at the internal ω atoms.

Thus, one can expect that the most active surface sites for the formation of the chemical bonds with the species having unpaired electrons are the ε and β sites in the ground state, and the γ and β sites in all the remaining states. Taking into account the Boltzman averaging of the spin densities among the four low-lying spin states, one can express the "activity" of the surface sites in the covalent bond formation with the adsorbed species as a series

$$\varepsilon > \gamma, \beta > \delta, \alpha$$

As it will be shown below, this sequence is in a qualitative agreement with the adsorption properties of the surface sites of Pt_{24}.

Bond Length Distribution. It was mentioned above that the Pt_{24} cluster has similar structural features in all the low-lying spin states ($M = 3, 5, 7, 9$). However, the fine differences in the bond lengths are remarkably different. There are also some small differences in the bond lengths within the same spin state. The main feature is the existence of three groups of bonds. Figure 4 demonstrates the bond length distribution in the four low-lying spin states of Pt_{24}. As is evident from the figure, there are three rather distinct groups of bonds—shortened (bond length in the range 2.70−2.80 Å), "normal" (2.8−2.95 Å), and

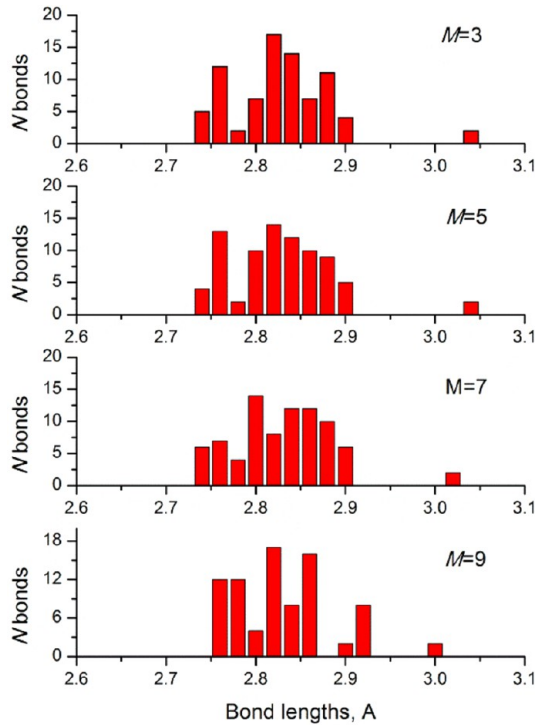

Figure 4. Bond length distribution in the optimized structures of Pt_{24} for the four low-lying spin states.

elongated (3.00−3.10 Å). Figure 5 demonstrates the positions of these bond groups in the cluster structure.

The elongated bonds (marked by dotted blue lines in Figure 5) are the $\varepsilon-\varepsilon$ interatomic distances, which should be equivalent to the $\delta-\delta$ distances in an ideal crystal. However, in the Pt_{24} cluster, the $\varepsilon-\varepsilon$ and $\delta-\delta$ distances are significantly different because of the remarkable displacement of ε atoms out of ($\beta\gamma\delta$) planes (the (111) faces of an ideal crystal).

The shortened bonds (marked in Figure 5 by the red bold lines) are formed by the different atoms due to the favorable electron coupling. As a rule, these are the bonds of α atoms with their neighbors and the atoms on the opposite sides of hexagonal faces corresponding to the (111) hexagonal planes. In the last case, the distortion of the ideal hexagons $\beta\beta\delta\gamma\gamma\delta$ in the states $M = 3, 5, 7$ appears due to the shortening of a bond pair in a single direction $\beta\varepsilon\gamma$, whereas two bond pairs are shortened in the directions $\beta\varepsilon\gamma$ for the state $M = 9$. Additionally, the $\beta-\beta$ bonds are remarkably shortened in two low spin states ($M = 3, 5$).

DOI: 10.1021/acs.jpcc.6b04555
J. Phys. Chem. C 2016, 120, 18570−18587

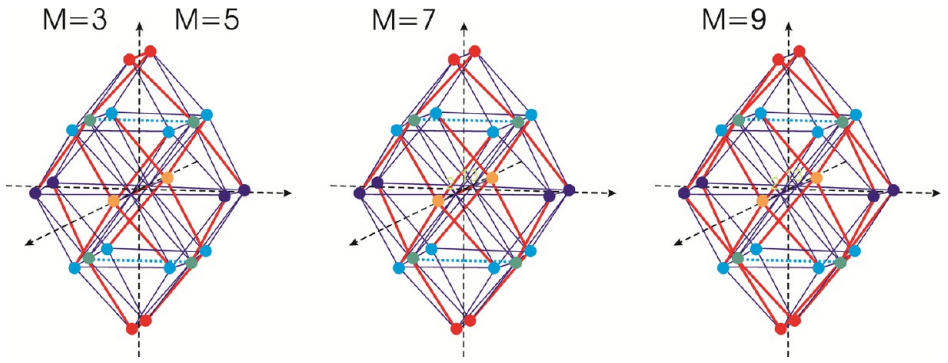

Figure 5. Bond length types of Pt_{24} in the low-lying spin states. Similar bond lengths are designated by the same color (bold red, shortened bonds; dotted blue, elongated bonds). The bond lengths in triplet and quintet states are close to each other.

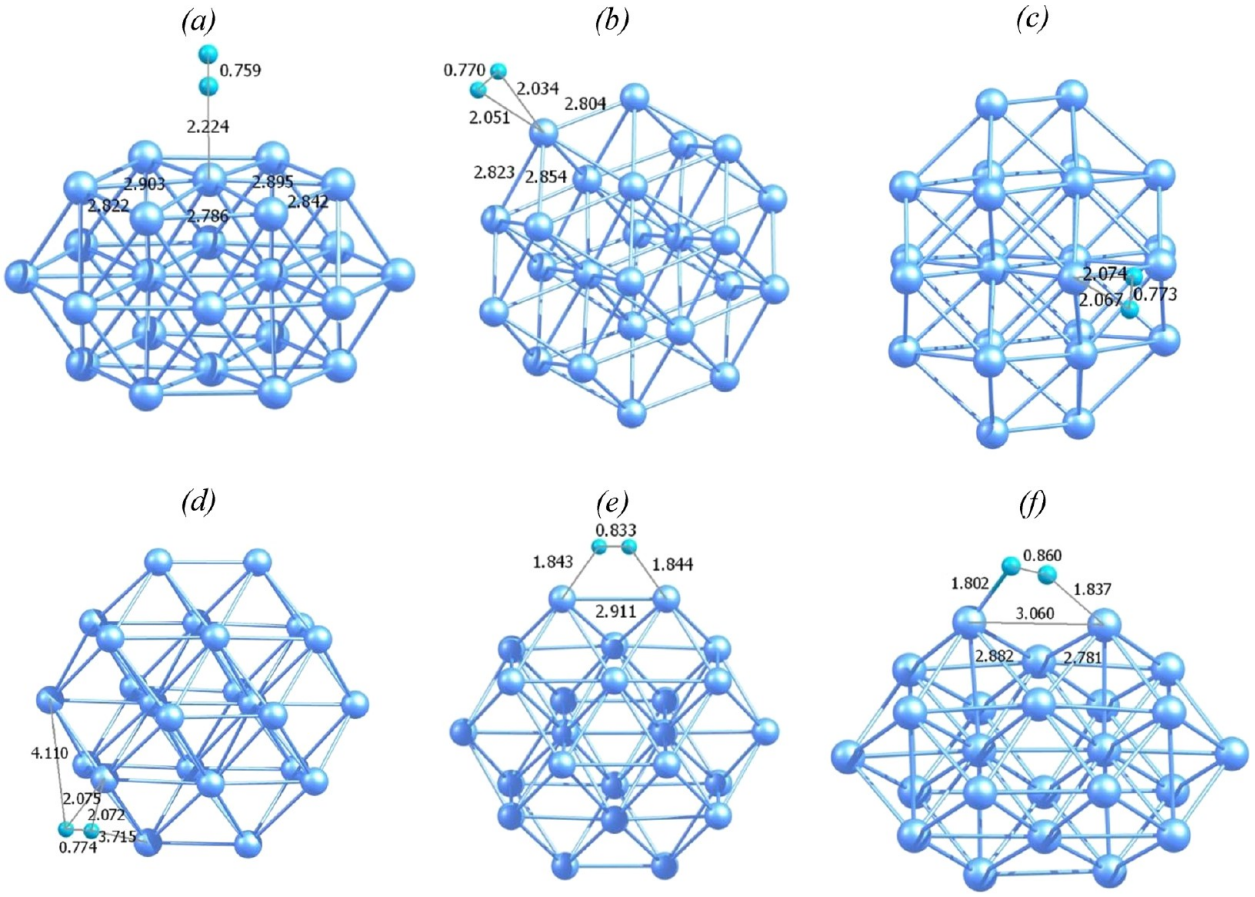

Figure 6. Optimized structures of coordination complexes of the molecular hydrogen at various surface sites of Pt_{24}: (a) T_{ε}; (b) L_{β}; (c) L_{γ}; (d) L_{δ}; (e) $B_{\beta\beta}$; (f) $B_{\gamma\gamma}$.

As a whole, the bond length differences between the shortened and "normal" bonds are not very pronounced and these two bond groups form rather compact distributions in the histograms (Figure 4). The elongation of $\varepsilon-\varepsilon$ distances does not violate the D_{2h} symmetry. These facts allow describing the symmetry of the Pt_{24} cluster approximately by the D_{2h} symmetry group.

It should also be mentioned that the energy differences between the idealized (D_{2h} optimized) geometry and slightly distorted structures in various spin states are quite small. For example, the D_{2h} optimized structure (most corresponding to the ideal crystal lattice structure) is only 0.3 kcal/mol higher in energy than the fully optimized quintet spin state. This difference is twice lower than the thermal energy (RT) at 300 K.

Physical Adsorption of Molecular Hydrogen. The similarities of the energies and properties of four low-lying spin states allow considering the adsorption of molecular hydrogen on the single state of the cluster only. Therefore, all the adsorption complexes corresponding to the molecular hydrogen coordination described here were located for the system in the quintet spin state (M = 5).

The first step of the hydrogen interaction with the Pt_{24} particle is a physical adsorption of molecular hydrogen. The full geometry optimization carried out from various starting points shows that only three modes of molecular hydrogen adsorption

DOI: 10.1021/acs.jpcc.6b04555
J. Phys. Chem. C 2016, 120, 18570−18587

Table 2. Calculated Energies $\Delta_{ads}E$, Enthalpies $\Delta_{ads}H^0$, and Gibbs Free Energies $\Delta_{ads}G^0$ (kcal/mol) for the Different Modes of the Hydrogen Adsorption on the Pt_{24} Cluster at Various Temperatures

site/mode	N_{sites}	$\Delta_{ads}E$	$\Delta_{ads}H^0$(0 K)	$\Delta_{ads}H^0$(298 K)	$\Delta_{ads}G^0$(298 K)	$\Delta_{ads}H^0$(500 K)	$\Delta_{ads}G^0$(500 K)
			H_2 Adsorption ($Pt_{24} + H_2 \rightarrow Pt_{24}{\cdot}H_2$)				
T_ε	4	−1.36	−0.07	−0.49	5.75	−0.02	9.85
L_β	4	−5.72	−3.91	−4.71	2.59	−4.42	7.45
L_γ	4	−4.50	−2.99	−3.58	2.82	−3.23	7.06
L_δ	8	−4.78	−3.13	−3.80	2.95	−3.47	7.45
$B_{\beta\beta}$	2	−6.67	−5.07	−6.20	1.37	−6.14	6.49
$B_{\gamma\gamma}$	2	−5.85	−4.39	−5.67	2.38	−5.65	7.84
averaged		−4.57	−2.99	−3.72	3.16	−3.42	7.74
			H Adsorption ($Pt_{24} + {}^1/_2H_2 \rightarrow Pt_{24}{\cdot}H$)				
$\gamma\gamma\varepsilon$ (FCC)	4*	−11.44	−10.97	−11.91	−6.72	−12.00	−3.16
$\gamma\delta\varepsilon$ (HCP)	8*	−7.84	−7.40	−8.26	−3.99	−8.36	−1.06
$\beta\delta\varepsilon$ (FCC)	8*	−9.14	−8.57	−9.50	−4.48	−9.62	−1.03
$\beta\beta\varepsilon$ (HCP)	4*	−7.85	−7.69	−8.46	−4.65	−8.53	−2.04
$\beta\delta\delta$	4	−8.29	−7.71	−8.66	−4.32	−8.80	−1.31
$\alpha\delta\delta$	4	−4.75	−4.53	−5.28	−1.36	−5.34	1.33
$\alpha\delta$	8	−5.21	−4.49	−5.19	−1.18	−5.32	1.59
$\delta\gamma$	8	−8.51	−7.57	−8.41	−3.69	−8.57	−0.44
$\beta\beta$	2	−8.94	−7.71	−8.63	−3.22	−8.82	0.50
ε	4*	−0.81	0.08	−0.51	4.20	−0.48	7.38
averaged		−7.33	−6.72	−7.54	−3.05	−7.65	0.04
Pt(111) averaged[a]		−7.72	−7.22	−8.06	−3.44	−8.14	−0.29
			H Subsurface Incorporation ($Pt_{24} + {}^1/_2H_2 \rightarrow Pt_{24}{\cdot}H$)				
$\varepsilon\varepsilon\omega\omega$	2	−6.02	−6.26	−6.90	−2.80	−6.86	−0.03
$\beta\beta\varepsilon\varepsilon$	4	−3.21	−3.05	−3.79	−0.16	−3.85	2.34
averaged		−4.15	−4.12	−4.83	−1.04	−4.85	1.55

[a]Averaged among the sites located at the Pt(111) microfacet (the sites marked by asterisks in the second column).

are feasible—on-top adsorption on single ε atoms (the coordination complex referred to hereinafter as T_ε), bridge-like adsorption on $\beta-\beta$ and $\gamma-\gamma$ atom pairs ($B_{\beta\beta}$, $B\gamma\gamma$), and the 2-fold (lateral) H_2 coordination on a single Pt atom which takes place at the β, γ, δ vertices of the cluster (L_β, $L\gamma$, L_δ). Figure 6 shows the typical examples of these coordination modes.

It should be stressed that we tried to find the bridge-like adsorption complexes of H_2 starting from several initial points including bridge-like structures of $\beta-\varepsilon$, $\gamma-\varepsilon$, and $\delta-\varepsilon$ types. The starting Pt−H distances were approximately 2.0−2.5 Å. In all of these cases, the optimization resulted in the 2-fold coordinated structures on single atoms. The initial coordination of H_2 in the region of the $\alpha\delta\gamma\delta$ square resulted in the dissociative adsorption (see below).

The energies of the located adsorption complexes of H_2 are given in Table 2. As is evident from the table, the on-top coordination is the least favorable one; its adsorption energy is only about 1.4 kcal/mol. The lateral coordination is more favorable with adsorption energies in the range 4.5−5.7 kcal/mol. The most favorable coordination is the bridge-like one with the energy of adsorption estimated as 5.9−6.7 kcal/mol.

It is interesting that the bridge-like adsorption complexes of the $B_{\beta\beta}$ and $B_{\gamma\gamma}$ kinds are significantly distinguished in their structures. The $B_{\beta\beta}$ complex is highly symmetric with two virtually equivalent H atoms. In contrast, the structure of the $B_{\gamma\gamma}$ complex is essentially asymmetric with the H_2 molecule twisted and tilted relative to the Pt−Pt bond. The minimum Pt−H distance (1.802 Å) in this case is much shorter than the distances in the $B_{\beta\beta}$ complex (1.844 Å). The maximum Pt−H distance of the $B_{\gamma\gamma}$ complex (1.837 Å) is also shorter than Pt−H in the $B_{\beta\beta}$ complex. Nevertheless, the $B_{\beta\beta}$ complex is remarkably more favorable in energy (6.67 kcal/mol) than the $B_{\gamma\gamma}$ one (5.85 kcal/mol). This is probably because of breaking of the Pt−Pt bond between two γ atoms taking place in the $B_{\gamma\gamma}$ complex. The $\gamma-\gamma$ distance is increased here to 3.060 Å, whereas the $\beta-\beta$ coordination leads to only slight elongation of the $\beta-\beta$ bond. At the same time, the H−H bond in the $B_{\gamma\gamma}$ complex is strongly elongated (0.860 Å) in comparison with the symmetric $\beta-\beta$ complex (0.838 Å) and especially with the free H_2 molecule (0.747 Å). This is evidence that the $\gamma-\gamma$ adsorption is very favorable to the farther dissociation of the H_2 molecule occurring at this adsorption site.

Dissociative Adsorption of Molecular Hydrogen. As was mentioned before, the optimization started from the initial position of H_2 over the $\alpha\delta\gamma\delta$ square (both for $\alpha-\delta$ and $\alpha-\gamma$ orientations of the H_2 molecule in parallel to the square plane at a distance of about 2.0 Å), resulting in the dissociation of the H_2 molecule and formation of two bridge-like coordinated H atoms either in the $\alpha-\delta$ and $\delta-\gamma$ positions or in two $\delta-\gamma$ ones; see Figure 7a. Both of the pathways of dissociative adsorption are activationless, but the final structures are slightly different in energy. The adsorption energy of two $\delta-\gamma$ coordinated H atoms relative to the quintet spin state of the $Pt_{24} + H_2$ system is 17.8 kcal/mol, which is 1.7 kcal/mol higher than in the case of dissociation to the pair of $\alpha-\delta$ and $\delta-\gamma$ coordinated hydrogen atoms.

Surface Dissociation and Surface Migration of Adsorbed Atom Pairs. The formation of the $\gamma-\gamma$ adsorption complex of molecular hydrogen with the strongly loosened structure of the H−H bond is very favorable for the dissociation of the H_2 molecule. The located structure of the transition state of such dissociation is shown in Figure 7b. The activation energy of the dissociation relative to the $\gamma-\gamma$ complex is only 2.29 kcal/mol (see Table 2), and the energy of the

DOI: 10.1021/acs.jpcc.6b04555
J. Phys. Chem. C 2016, 120, 18570−18587

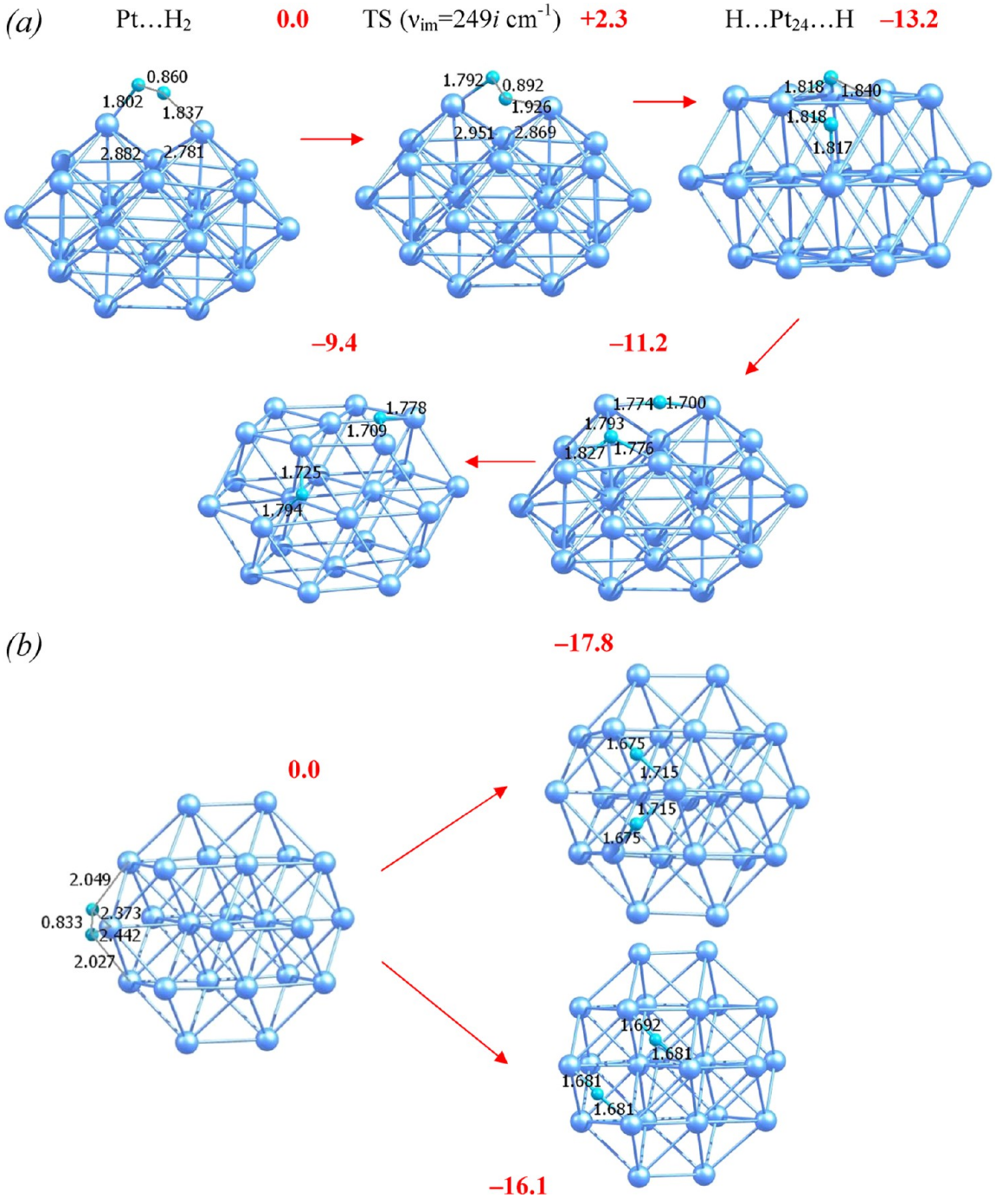

Figure 7. Optimized structures of (a) the molecular hydrogen dissociation pathway proceeding from the $B_{\gamma\gamma}$ complex resulting in the formation of the pair of complexes $\gamma\gamma\varepsilon + \gamma\delta\varepsilon$ and (b) two activationless dissociation pathways resulting in the formation of the pair of the complexes $\gamma\delta + \gamma\delta$ or $\gamma\delta + \alpha\delta$. Red bold values are the relative energies in kcal/mol.

transition state is about 3.6 kcal/mol lower than the energy of the ground state of the Pt_{24} + H_2 system. Thus, although the adsorption at the γ–γ site has formally an activated barrier, the barrier height is lower than the adsorption energy and the gross process is also activationless.

The intrinsic reaction coordinate (IRC) procedure performed in both directions from the located transition state converges to the γ–γ complex and to the new structure with a pair of H atoms coordinated at both sides of the γ–γ bond in the $\gamma\gamma\varepsilon$ regions of the Pt_{24} cluster (see Figure 7). The energy of such dissociation is −19.1 kcal/mol relative to the free Pt_{24} and H_2 reagents (−13.2 kcal/mol relative to the γ–γ complex). It is interesting that the surface migration of the hydrogen atom pair from the γ–γ site to the other position on the surface requires a rather remarkable energy increase. For example, the migration of each atom from the $\gamma\gamma\varepsilon$ triangular region at the γ–γ site to the neighboring $\gamma\delta\varepsilon$ triangular region results in approximately 2 kcal/mol of the energy increase (see Figure 7b). Such a remarkable variation of the energy during the atom pair migration requires a special consideration of the H atom adsorption.

DOI: 10.1021/acs.jpcc.6b04555
J. Phys. Chem. C 2016, 120, 18570–18587

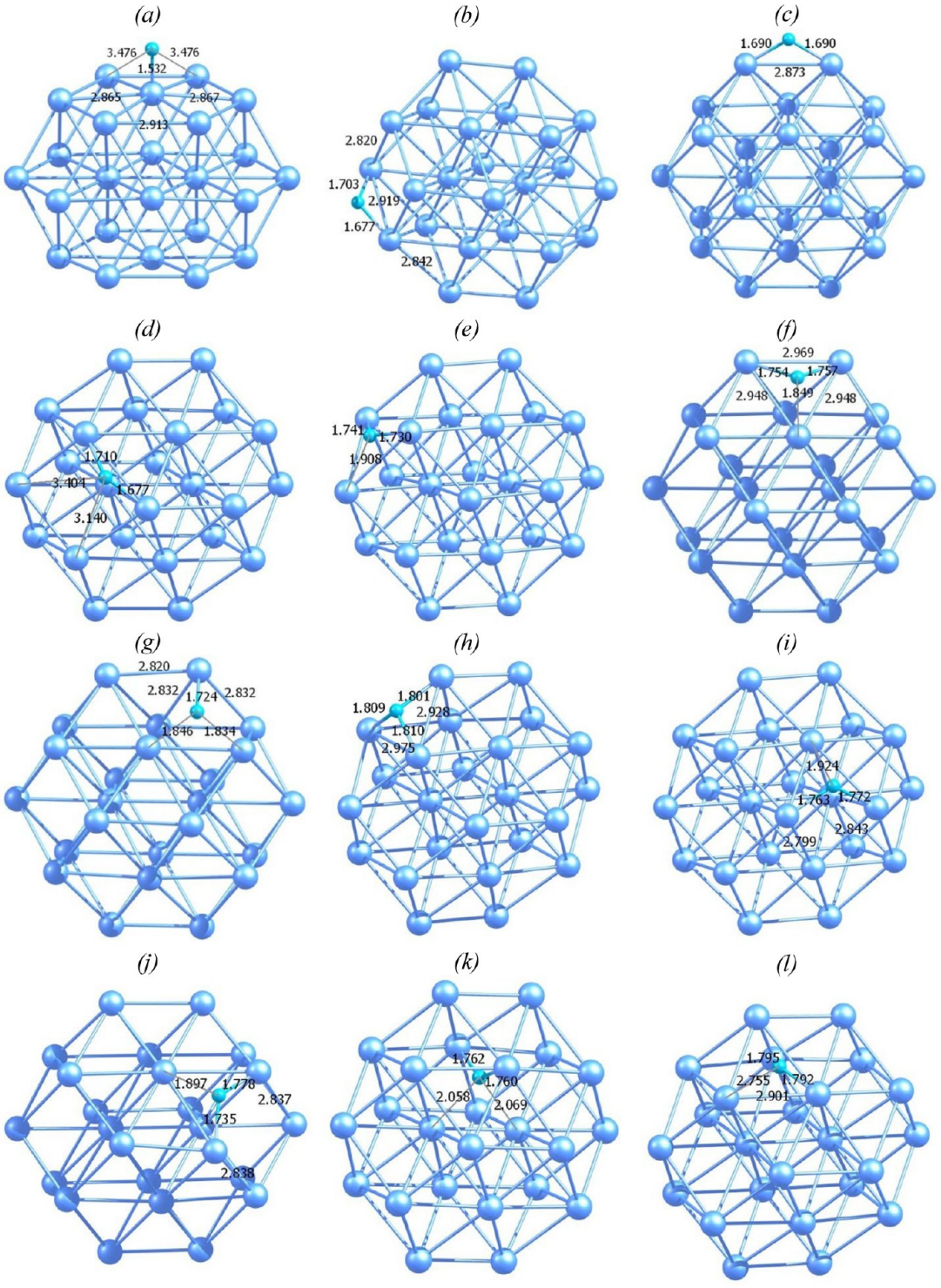

Figure 8. Optimized structures of coordination complexes of the atomic hydrogen at various surface sites of Pt_{24} and inside the cluster: (a) ϵ; (b) $\alpha\delta$; (c) $\beta\beta$; (d) $\delta\gamma$; (e) $\alpha\delta\delta$; (f) $\beta\beta\epsilon$; (g) $\beta\delta\epsilon$; (h) $\beta\delta\delta$; (i) $\gamma\gamma\epsilon$; (j) $\gamma\delta\epsilon$; (k) $\epsilon\epsilon\omega\omega$; (l) $\beta\beta\epsilon\epsilon$.

Adsorption of Atomic Hydrogen and Its Surface Migration. The strong variation of the energies of hydrogen atoms coordinated at the different surface sites requires a special consideration of the adsorption complexes at the surface of the Pt_{24} particle. Because the free electron of the H atom should effectively couple the free valence of Pt_{24} in its ground (quintet) state, we considered the formation of $Pt_{24}\cdots H$ complexes in its quartet spin state.

The high symmetry (D_{2h}) of the Pt_{24} cluster makes it possible to map the energy of adsorption for the whole surface of the subnanoparticle. Figure 8 shows the optimized structures of various coordination complexes of atomic hydrogen at Pt_{24}. Figure 9 shows the adsorption energy map for the $Pt_{24}\cdots H$ system in the quartet spin state for all the unique regions of the Pt_{24} cluster possessing D_{2h} symmetry. The colored circles designate the unique atoms of Pt_{24}, and the solid black lines correspond to the Pt−Pt bonds (edges of the cluster). The

DOI: 10.1021/acs.jpcc.6b04555
J. Phys. Chem. C 2016, 120, 18570−18587

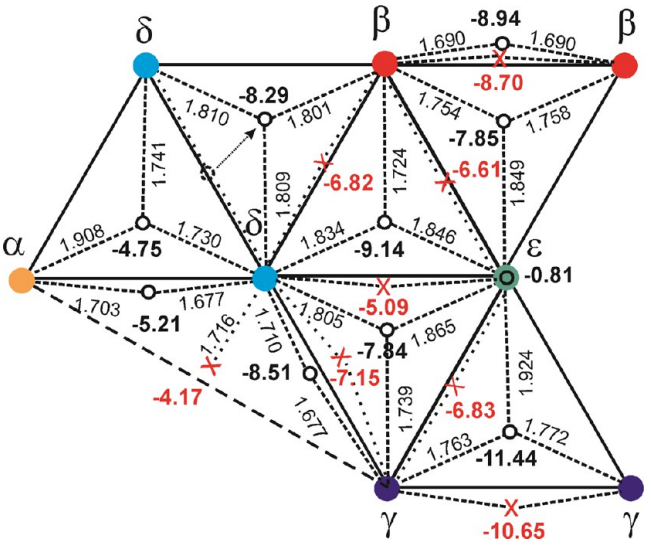

Figure 9. Calculated map of the H atom adsorption energies for the unique surface regions of Pt_{24}. The open circles show the local minima, and the red crosses, the surface migration transition states.

open black circles mark the positions of the located adsorption minima of H atoms at the surface of the cluster, and the dashed lines show the shortest distances to the surface Pt atoms. The red crosses show the located transition states of the surface migration of adsorbed H atoms between the surface local minima, and the dotted lines give the distances from them to the closest Pt atoms.

It was found that the on-top coordination of the H atom is possible only at the ε Pt atom and the corresponding adsorption energy is very low, only 0.8 kcal/mol. Nevertheless, this adsorption complex is a true local minimum with all positive vibrational frequencies. We failed to locate the similar on-top coordination complexes on all the remaining unique surface atoms in spite of many attempts to start optimization from different starting positions. This fact stays in a sharp distinction from the results obtained earlier with the periodic cluster calculations.

The average adsorption energy accounting for the number of various sites can be calculated using the formula

$$\langle E \rangle = \sum_i g_i E_i / \sum_i g_i \qquad (1)$$

where g_i is the number of adsorption sites i on the Pt_{24} surface and E_i is the relative adsorption energy of site i measured from the energy level of the most favorable adsorption site ($\gamma\gamma\varepsilon$). The average adsorption energy for the H atom coordination is 7.33 kcal/mol. The corresponding average value for the molecular hydrogen adsorption is 4.57 kcal/mol, and it is 4.15 kcal/mol for the subsurface coordination of the H atom. Additionally, we used the Boltzman averaging

$$\langle E_T \rangle = \frac{\sum_i g_i E_i \exp(-E_i/RT)}{\sum_i g_i \exp(-E_i/RT)} \qquad (2)$$

to estimate the thermally averaged adsorption energy. It is obvious that eq 2 becomes equivalent to eq 1 in the limit of infinite temperatures. If $T = 0$, eq 1 reduces to the minimum E_i value (E_{min}). Thus, the $\langle E \rangle$ and E_{min} values shown in Table 2 represent the higher and lower borders for the thermal averages of binding energies and enthalpies which can be directly compared to the experimental values measured at the given temperature.

As was mentioned above, there are only seven unique regions of the Pt_{24} cluster of D_{2h} symmetry. The adsorption complexes of 3-fold coordinated H atoms were found in all of these regions except for the $\alpha\gamma\delta$ one. In the last case, only 2-fold bridge-like coordinated structures were located at the α–δ and

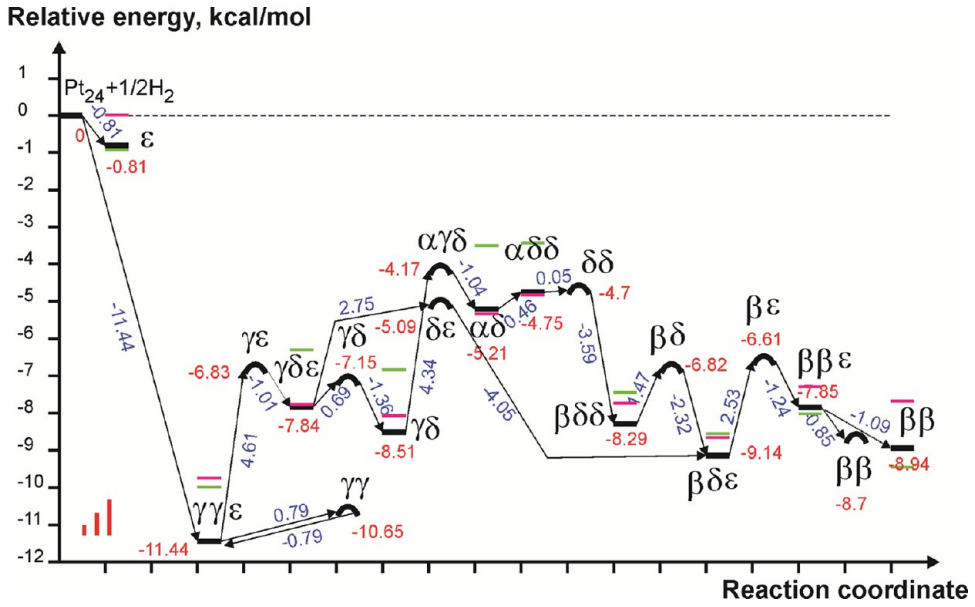

Figure 10. PES profile for the surface migration of the H atom on the surface of the Pt_{24} cluster. Greek letters, their pairs, and their triples designate the positions of mono-, bi-, and three-coordinated H atoms, respectively. Black bars correspond to the quartet spin states, whereas green and magenta bars, to the doublet and sextet spin states, respectively. Horizontal (red) values designate the energy of the adsorption complexes and transition states in the quartet spin state relative to the initial Pt_{24}(quintet) + $^1/_2H_2$ system. The tilted (blue) values are the transition energies between the stationary points. All values are in kcal/mol. Vertical red bars in the left bottom corner indicate the thermal energy (RT) for temperatures of 100, 300, and 500 K.

DOI: 10.1021/acs.jpcc.6b04555
J. Phys. Chem. C 2016, 120, 18570−18587

$\gamma-\delta$ cluster edges corresponding to the structures formed during the dissociative adsorption described above. Another bridge-like structure was found at the $\beta-\beta$ cluster edge. It should be noted that we failed to find the analogous bridge-like structure on the $\gamma-\gamma$ site as well as at the other Pt−Pt surface bonds. It can be due to the fact that the bridge-like structures are favorable only in the case when the dihedral angle of the Pt−Pt edge between two adjacent triangular regions is higher than some limiting value. In the case of the $\beta-\beta$ edge, this dihedral angle is about 75°. In the cases of $\alpha-\delta$ and $\gamma-\delta$ edges, these angles are 70 and 71°, respectively, whereas the $\gamma-\gamma$ edge is characterized by the corresponding angle of 111° and this value is even higher for all the remaining cluster edges. Thus, the limiting value of the dihedral angle allowing the bridge-like coordination lies between 75 and 111° (the bridge-like coordination is allowed at the lower values of this angle).

As is evident from Figure 9, the adsorption energies of 2- and 3-fold coordinated H atoms are in the range of 4.8−11.4 kcal/mol. The most energetically favorable adsorption site is the $\gamma\gamma\varepsilon$ region, whereas the least favorable one is the $\alpha\delta\delta$ region. It is interesting that the 3-fold coordinated $\alpha\delta\delta$ adsorption complex (4.75 kcal/mol) is less favorable than the adjacent 2-fold coordinated one at the $\alpha-\delta$ edge (5.21 kcal/mol). It should also be noted that the bridge-like $\beta-\beta$ complex (8.94 kcal/mol) is more favorable than the neighboring 3-fold coordinated $\beta\beta\varepsilon$ site (7.85 kcal/mol).

The experimental values for the thermodynamic quantities of the hydrogen adsorption on metal surfaces are extremely influenced by the crystallite size, the method of the metal surface pretreatment, and the support type used for the metal deposition. For the enthalpy of adsorption, the experimental values are typically varied from 2 to 20 kcal/mol (for the adsorption process Pt(s) + $^1/_2H_2$).[69,70] Thus, the direct comparison of the calculated and experimental data is quite difficult. Anyway, the averaged H adsorption enthalpy for the Pt(111) microfacets at the standard temperature in Table 2 (−8.06 kcal/mol) is in good agreement with the reported experimental data of Sen et al.:[70] 6.5−7.5 kcal/mol for 2% Pt/TiO_2 with 1.6−2.4 nm crystallite size, 8.0 kcal/mol for 2.1% Pt/Al_2O_3 (2.7 nm), 8.5 kcal/mol for 2.1% Pt/SiO_2 (4.5 nm).

In accordance with the well-known classification of three-coordinated (hollow) sites of the ideal Pt(111) surface, the $\gamma\gamma\varepsilon$ and $\beta\delta\varepsilon$ regions of Pt_{24} can be designated as FCC (face-centered cubic) sites, whereas the $\gamma\delta\varepsilon$ and $\beta\beta\varepsilon$ regions are the HCP (hexagonal closest packing) ones. There are many studies demonstrating that the FCC sites are usually more favorable in coordination energy than HCP ones (see the Discussion below). Our results stay in agreement with these data giving the 1.3−3.6 kcal/mol higher adsorption energy for the FCC sites.

The migration of the H atoms on the Pt_{24} surface requires a rather remarkable activation energy. To estimate it, we considered the migration of the H atom formed from the Pt_{24}(quintet) + $^1/_2H_2$ system via different routes on the Pt_{24} surface. Figure 10 shows the energy diagram for such a migration.

The bold horizontal bars in Figure 10 indicate the local minima, and the bold arcs, the located transition states between them. The first steps are the formation of the ε-coordinated on-top complex and the most favorable three-coordinated $\gamma\gamma\varepsilon$ complex. Because the ε complex is essentially a metastable state, we do not consider its rearrangements in detail. The migration from the $\gamma\gamma\varepsilon$ complex is more interesting and occurs via three main channels shown by the sequences of solid arrows. The first one is a H transfer between two $\gamma\gamma\varepsilon$ sites located at different (111) faces. The other two channels begin by the $\gamma\gamma\varepsilon \rightarrow \gamma\delta\varepsilon$ transfer with subsequent branching shown in Figure 10. As is evident from the diagram, the high activation barriers (4.6 and 4.3 kcal/mol) take place for the transitions $\gamma\gamma\varepsilon \rightarrow \gamma\delta\varepsilon$ and $\gamma\delta \rightarrow \alpha\delta$. Among other transitions, $\gamma\delta\varepsilon \rightarrow \beta\delta\varepsilon \rightarrow \beta\beta\varepsilon$ (both at the (111) face of the cluster) have activation energies of 2.75 and 2.64 kcal/mol. Surprisingly, the transitions between different faces are less hindered. For example, the transition between two adjacent (111) faces through the $\gamma\gamma$ transition state has a barrier of only 0.79 kcal/mol. This is probably due to the high stability of the adsorption sites at the HCP site of the same face.

All of the estimated energy barriers are lower than the typical energy of adsorption at all the explored adsorption sites except the monocoordinated ε complex. Some of the barriers are lower than the barriers of the dissociation of H_2 on the surface (2.9 kcal/mol). However, the barriers of migration from the $\gamma\gamma\varepsilon$ and $\gamma\delta$ complexes are remarkably higher. Thus, the mobility of the H atom trapped in these positions is significantly decreased. This fact probably has an influence on the activation energy of the hydrogenation occurring at this surface site.

Effect of Spin Multiplicity Changes on the H Atom Adsorption Complexes. In order to estimate the effect of spin multiplicity on the structure and energy of adsorption complexes, we reoptimized the located H atom adsorption complexes in the doublet and sextet spin states using the quartet state geometry as starting points. The calculated structural parameters and absolute thermodynamic parameters are presented in the Supporting Information. The relative energies of the optimized complexes are presented in Figure 10 as green (doublet spin state) and magenta (sextet spin state) bars. As is evident from the calculation data, the influence of the spin state multiplicity is not significant although remarkable. The energy changes are in the range of 1.7 kcal/mol. In most cases, the quartet spin state remains to be the ground state. The only exceptions are $\alpha\delta\delta$ and $\alpha\delta$ complexes in the sextet state (lower by 0.1 kcal/mol than the sextet complexes) and ε, $\beta\beta\varepsilon$, and $\beta\beta$ complexes in the double state (lower in energy by 0.1, 0.2, and 0.5 kcal/mol than the corresponding sextet structure). In all of these cases, the optimized structures are essentially the same in all three spin states. On the basis of the presented data, we conclude that, as a whole, the changes in spin multiplicity do not change the PES profile presented in Figure 10. The calculated thermodynamic parameters presented in Table 2 can be corrected for the low-lying spin states assuming that the vibrational frequencies are close to the values obtained for the quartet spin state. As it follows from eq 2, the resulting average energies approach the lowest one if the energy differences between states are high and are located between two average values otherwise. Thus, on the basis of the proximity of the energies and structural parameters for low-lying spin states presented in Figure 10, we conclude that the multiplicity changes have only a slight effect on the thermodynamic parameters of the adsorption complexes.

Diffusion of Atomic Hydrogen inside the Cluster. Among the reaction channels of hydrogenation occurring at the supported NP catalysts, the spillover processes are frequently considered as possible mechanisms influencing the chemical rate and catalytic selectivity. The spillover at the oxide supported Pt NPs can include the transfer of the H atoms formed at the Pt NPs to the surface of the oxide support (SiO_2, TiO_2, Al_2O_3, etc.). It is obvious that the energy and the

DOI: 10.1021/acs.jpcc.6b04555
J. Phys. Chem. C 2016, 120, 18570−18587

activation barriers of such a transfer can be estimated as the energy of desorption of H atoms from the Pt_{24} cluster (which is estimated above) and further adsorption of them at the support surface. However, it is also interesting to estimate the possibility of the H atom transport from the Pt NP surface to the support surface via the internal diffusion of H atoms inside the nanoparticle. This process can be modeled by the H atom migration between the various centers inside the Pt_{24} cluster.

In order to do that, we optimized the structures of the H atoms inside all the internal polyhedra (tetrahedra, pyramides, and octahedra) of the Pt_{24} cluster. It was found that the H atoms located at the centers of all the surface polyhedra (i.e., polyhedra having the faces forming the surface of a cluster) do not form the complexes and go outside during the optimization. We conclude that the H atoms buried at the first surface layer go outside without an activation barrier. Only two stable positions were found during the optimization of the H atom inside the Pt_{24} cluster (see Figure 8).

The first one is the bridge-like position between the $\varepsilon-\varepsilon$ edges of the internal tetrahedron $\varepsilon\varepsilon\omega\omega$ (Figure 8k), which has no faces at the surface of the cluster. It is interesting that the H atom cannot be coordinated at the $\omega-\omega$ edge of this tetrahedron as well as at its center (moved out spontaneously to the $\varepsilon-\varepsilon$ structure). The energy of the $\varepsilon-\varepsilon$ complex is −6.02 kcal/mol relative to the Pt_{24} + $^1/_2H_2$ system. This energy is comparable with the energies of some adsorption sites, and this structure is even more favorable than the ε, $\alpha\delta$, and $\alpha\delta\delta$ adsorption complexes. The second local minimum of the H atom inside the Pt_{24} cluster is the similar complex of the $\varepsilon-\varepsilon$ bond but with the H atom located close to the $\beta\varepsilon\varepsilon$ plane of the $\beta\delta\delta\varepsilon\varepsilon$ pyramid (see Figure 8l). This structure is much less favorable with an energy of formation of only −3.21 kcal/mol. If we consider the energies of the located structures relative to the energy of the most favorable $\gamma\gamma\varepsilon$ complex as estimates for the barriers of subsurface diffusion, we obtain values of 5.42 and 8.23 kcal/mol, respectively.

On the basis of these energies, we conclude that the activation energy of the spillover process occurring via the subsurface diffusion of H atoms is comparable with the energy barriers of the surface migration and the "through-space" transfer of H atoms to the catalyst support. In some cases, when the surface migration is hindered (e.g., by the ligands strongly adsorbed at the Pt NP surface), this can provide the effective channel of the H transport to the support surface or to the other free sites at the Pt NP surface. The activation barriers of such a transport are thus comparable to the activation energies of many reactions taking place at the surface of Pt NPs.

IR and Raman Spectra for Various Adsorption Complexes of Molecular Hydrogen. The vibrational frequencies of the initial Pt_{24} clusters are located in the region lower than 200 cm^{-1}. The M = 3, 5, 9 states have three rather distinct features close to 80, 100−120, and 160 cm^{-1}. At the same time, the M = 7 state is characterized by only two structureless bands at 80−100 cm^{-1} (higher intensity) and 150−160 cm^{-1} (lower intensity). As a whole, the IR spectra of all the considered spin states are only slightly different and all the bands have extremely low intensities (typically lower than 1 km/mol). Thus, it is quite unlikely that the Pt_{24} spin states can be registered and distinguished using the IR spectroscopy.

In contrast, the IR spectra of T, L, and B complexes of molecular hydrogen formed at the Pt_{24} surface are rather remarkably distinguished (see Figure 11a). The $T_{\varepsilon\varepsilon}$ complex is characterized by the very intense H_2 stretching band near 4000

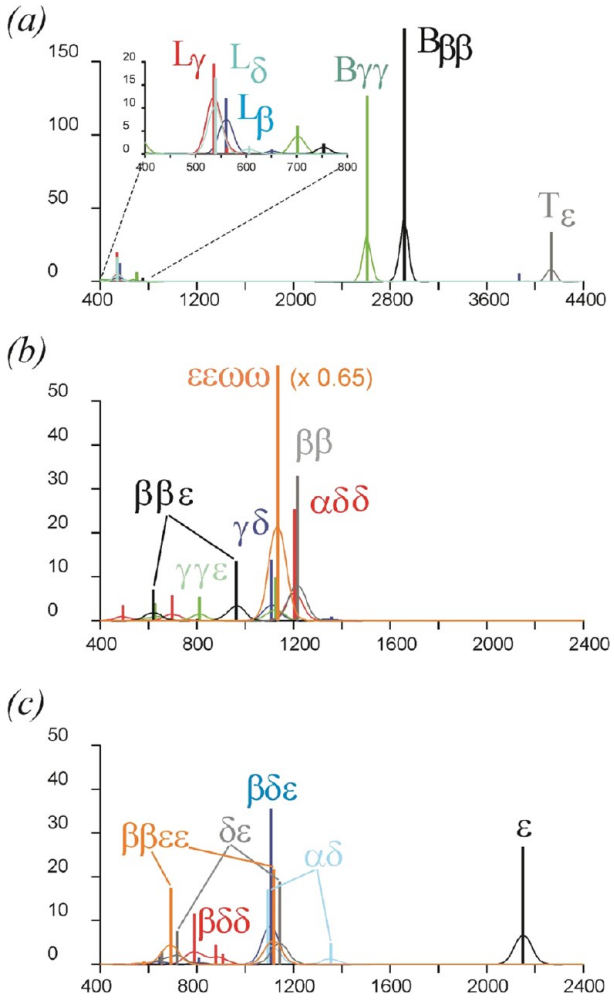

Figure 11. Calculated IR spectra of the most favorable coordination complexes formed between molecular and atomic hydrogen and the Pt_{24} cluster: (a) complexes of $Pt_{24}{\cdot}H_2$ (M = 5); (b, c) surface and subsurface coordination complexes of $Pt_{24}{\cdot}H$ (M = 4) (intensity of $\varepsilon\varepsilon\omega\omega$ is scaled by 0.65). Vibrational frequencies are not scaled. The horizontal axis is wavenumber in cm^{-1}, and the vertical axis is IR intensity in km/mol.

cm^{-1}. Its unscaled calculated harmonic frequency is 4136 cm^{-1} (IR intensity 34 km/mol), whereas the calculated at the same theory level harmonic frequency of the free H_2 molecule is 4393 cm^{-1} (the calculated Raman activity of this vibration is 67.9 $Å^4$/amu). Thus, the red shift of the vibrations of molecular hydrogen coordinated at the T_ε site (red shift of 257 cm^{-1}) can be in principle registered using the combination of the IR and Raman spectroscopy. The IR intensities of H−H stretching of the L-type complexes are characterized by frequencies below 4000 cm^{-1}, and their IR intensities are quite low. The only exception is the $L_{\beta\beta}$ complex where the H−H stretching band at 3870 cm^{-1} has an intensity of 5.5 km/mol, approximately 1 order of magnitude higher than for other L-type complexes with unscaled harmonic frequencies of 3930 cm^{-1} (L_δ) and 3937 cm^{-1} (L_γ). The most pronounced spectral features of the molecular adsorption complexes take place in the case of bridge-like complexes. They are characterized by the intense bands of extremely red-shifted H−H stretchings (2917 cm^{-1}, 173 km/mol in the case of $B_{\gamma\gamma}$ and 2610 cm^{-1}, 126 km/mol in the case of $B_{\beta\beta}$). The extremely high red shifts (1476 and 1783 cm^{-1}) are evident that the covalent bond of the H_2 molecule is

DOI: 10.1021/acs.jpcc.6b04555
J. Phys. Chem. C 2016, 120, 18570−18587

significantly activated and near a dissociation. The comparison of the calculated red shifts of molecular complexes supports the conclusion that the formation of the bridge-like complexes along with dissociative adsorption on $\alpha\delta$ or $\gamma\delta$ sites (see above) are the main channels of the H_2 dissociation at the Pt_{24} surface.

The corresponding calculated Raman activities are shown in Figure 12a. It is seen that the most intense peak for the T_ε complexes is located near 4000 cm^{-1}. All three L complexes are characterized by slightly lower scattering frequencies in the range 3700−3800 cm^{-1}. At the same time, bridge-like complexes are characterized by the lower but still intense scattering bands in the range 2700−2900 cm^{-1}. There are also lower frequency bands of these complexes in the region 400−800 cm^{-1}. However, the intensities of these bands are much lower, which makes their registration difficult.

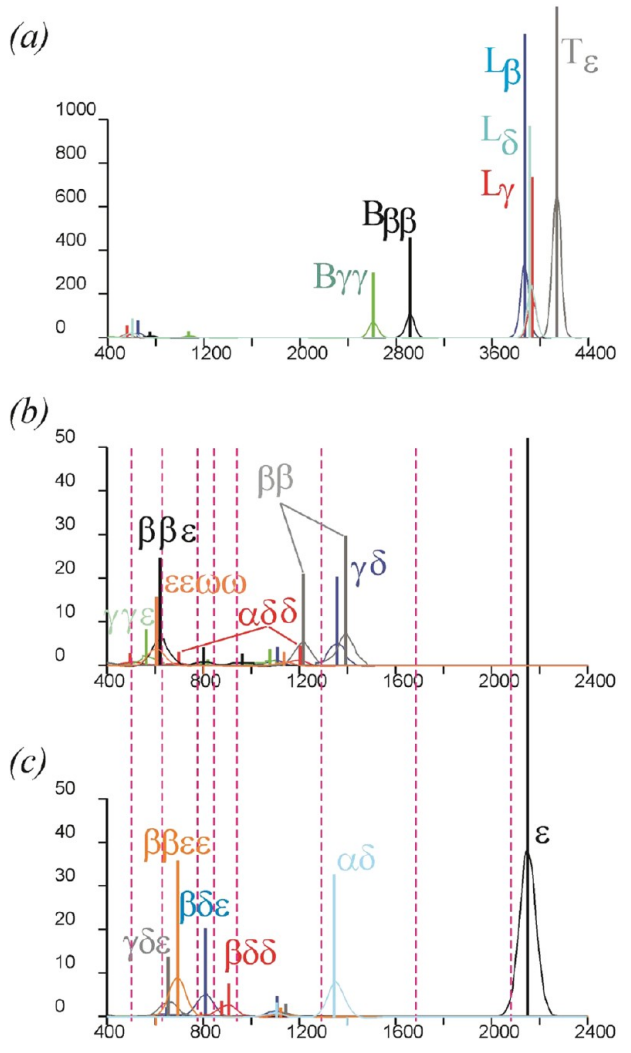

Figure 12. Calculated Raman scattering activities of the most favorable coordination complexes formed between molecular and atomic hydrogen and the Pt_{24} cluster: (a) Complexes of $Pt_{24}{\cdot}H_2$ (M = 5) (activity of T_ε is scaled by 0.5); (b, c) Surface and subsurface coordination complexes of $Pt_{24}{\cdot}H$ (M = 4). The horizontal axis is wavenumber in cm^{-1}, and the vertical axis is Raman scattering activity in $Å^4$/amu. Vibrational frequencies are not scaled. Vertical pink dashed lines are the band positions of experimental Raman spectra (RAIRS) and inelastic neutron scattering (IINS) of hydrogen deposited on Pt from ref 72.

IR and Raman Spectra of H Atoms Coordinated at the Pt_{24} Surface. The IR spectra of H atoms coordinated on the Pt_{24} cluster can be divided into three groups. The first one is the spectra of 2-fold coordinated atoms shown in Figure 11a. They contain two vibrations in the region 1100−1500 cm^{-1} with at least one intense band which is located usually in the region 1100−1200 cm^{-1}. It is interesting that the more intense band corresponds to the deformation vibration of the H atom perpendicular to the Pt−H−Pt bond plane, whereas the antisymmetric stretching of this bond is much less intense.

The second group of IR spectra corresponds to the vibrations of the three-coordinated surface H atoms and contains three IR bands distinguished in their positions and intensities (see Figure 11b,c). The most energetically favorable adsorption complex $\gamma\gamma\varepsilon$ is characterized by three equidistant bands in the region 500−1100 cm^{-1} of approximately equal intensity. The same pattern takes place also for the same complex in the spin states M = 2 and 6. At the same time, the $\beta\delta\varepsilon$ complex is characterized by a similar pattern with strong nonequality of the band intensities (the high-frequency band near 1100 cm^{-1} is much more intense than the two others). The $\gamma\delta\varepsilon$ and $\beta\delta\delta$ complexes are significantly distinguished by their IR band patterns (see Figure 11b). It should also be noted that the one-fold coordinated ε complex and two located structures of H atoms buried inside the Pt_{24} have also rather distinguished IR band patterns, as is shown in Figure 11. These results are in good agreement with the experimental data obtained for the H_2 adsorption on the ideal Pt(111) surface at the coverage close to 1 ML;[71] see also ref 24. It was found that the IR band near 900 cm^{-1} appears after the H adsorption on FCC sites.

The corresponding calculated Raman scattering activities are shown in Figures 12b,c along with the available experimental data[72] for the hydrogen adsorbed on the Pt surface. As is evident from the figures, the Raman scattering allows rather clear distinguishing between different adsorption modes of surface and subsurface hydrogen. Almost all the calculated bands are located near the corresponding experimental band positions. The only exception is the experimental band near 1700 cm^{-1} which can probably be assigned to the $\beta\beta$, $\gamma\delta$, or $\alpha\delta$ structures or to the on-top (ε-like) complex located on the surface planes different from (111). The main band position of the ε complex on the (111) microfacet of Pt_{24} is located in the region of the broad experimental band 2050−2250 cm^{-1}, but other microfacets formed on the polycrystallic platinum surface can result in significant decreasing of the vibration frequency. It is also noticeable that the least favorable ε complex has an extremely high scattering ability.

Thus, the remarkable differences in the IR and Raman band patterns of the complexes allow in principle the formed adsorption structures to be distinguished experimentally.

DISCUSSION AND COMPARISON WITH PREVIOUS STUDIES

The hydrogen adsorption energies and structures for many coordination complexes located in the present study are in good agreement with the available data, both theoretical and experimental. However, some results obtained here are quite different from the previous studies.

The values of the adsorption energy at the (111) facet estimated in our study as 7.9−11.4 kcal/mol are in good agreement with the adsorption energy of H_2 on the Pt(111) surface experimentally determined in ref 18 with the LEED,

DOI: 10.1021/acs.jpcc.6b04555
J. Phys. Chem. C 2016, 120, 18570−18587

ELS, TDS, and contact potential measurements (two adsorption states corresponding to the low and higher coverage with maximum activation energy of desorption of 9.5 kcal/mol). The average value of 8.88 kcal/mol obtained in our study for the adsorption energies on the Pt_{24} sites corresponding to the Pt(111) faces (see Table 2) is also in good agreement with the adsorption energy for sub-ML coverages of H atoms on Pt(111) measured in ref 19 on the basis of using the He beam diffraction technique (8.6 kcal/mol relative to the free H_2 molecule). Recently, the authors of ref 23 pointed out that the defect-free Pt(111) surface is low-active in the dissociative adsorption of H_2 which is also consistent with the results obtained in our work. For Pt powder on SiO_2 (Europt-1 catalyst), the differential heat of adsorption at the initial stage measured with different calorimetric techniques is 100 kJ/mol[73] which is in reasonable agreement with other studies of silica or zeolite supported catalysts with different Pt loadings[74] as well as with the value of 90 kJ/mol for unsupported prereduced Pt powder.[75] Available data were summarized in ref 26.

Our results are also in agreement with the results of ref 25 where the combined experimental and theoretical study of the hydrogen TPD spectra on the reconstructed Pt(110) surface has been performed. The H atom adsorption energy on the reconstructed (110) face ridge was estimated in this study in the range from 6.5 to 9.2 kcal/mol (depending on the coverage) per single H atom and as 5.3 kcal/mol for the FCC site of the (111) microfacet on the basis of the periodic calculations (the RPBE functional over the plane wave basis set). These values are close to the energies obtained by us for the bridge-like H complexes $\alpha\delta$, $\delta\gamma$, and $\beta\beta$ (5.2−8.9 kcal/mol), whereas the FCC value is significantly lower than the $\gamma\gamma\varepsilon$ and $\beta\delta\varepsilon$ energies on Pt_{24} (9.1−11.4 kcal/mol).

The adsorption energies of atomic hydrogen on the ideal Pt(111) surface (at 1/4 ML coverage) was estimated by Ford et al.[36] using the periodic calculations with the PW91 and RPBE functionals in the plane wave basis. The PW91/PWB adsorption energies (reduced to our initial state and units) are 7.88, 7.64, and 6.95 kcal/mol for the H adsorption on the top, FCC, and HCP sites, respectively. These values are close to our adsorption energy on the HCP site (7.84−7.85) but differ significantly from both of our values for the FCC (9.14 and 11.44) and ε sites (0.81 kcal/mol). Moreover, the on-top adsorption complex is a most favorable structure in ref 36, whereas our calculations show that the ε-complex is quite unfavorable. Probably, this is the consequence of the lateral interactions between neighboring atoms destabilizing the two- and three-coordinated complexes and, simultaneously, making the neighboring on-top structure more favorable due to the parallel orientations of the dangling Pt−H bond dipoles. This effect is absent in our calculations. It also cannot be excluded that the artificial stabilization of the on-top structures (the interactions between the ghost atoms of the nearest periodic images) took place due to the nonphysical interactions between the periodic surface slabs separated by 12 Å.

The on-top adsorption complexes were also found at the NP vertices in the periodic cluster DFT study of hydrogen adsorption on Pt−Au bimetallic nanoparticles.[34] The on-top adsorption energies were estimated as 6.39 kcal/mol for the single H atom adsorbed at the Pt_{85} vertex corresponding to the (100) plane. It should be noted that the authors used different methods for the adsorption energy calculations and the value of 5.43 kcal/mol was obtained for the adsorption of the pair of H atoms at the same NP. Also, the on-top adsorption complexes on the edges of the NP with the adsorption energies in the range from 9.4 to 10.4 kcal/mol per H atom were located. All of these binding energy values are much higher than the value obtained by us for the T_ε complex (0.8 kcal/mol). As mentioned above, we also failed to find the stable on-top structures on the edges and vertices of Pt_{24}.

Among the bridge-like adsorption complexes, the authors of ref 34 found three stable structures with the adsorption energies in ranges from 8.7 to 13.8 kcal/mol per atom. This is remarkably higher than the energies of 5.2−8.9 kcal/mol found in the present study for the bridge-like complexes $\alpha\delta$, $\delta\gamma$, and $\beta\beta$. It is noticeable that the authors of ref 34 found three bridge-like structures (B1, B4, and B6 in the notation of ref 34) corresponding to $\beta\delta$ and $\gamma\varepsilon$ which are not the local minima at Pt_{24}. Among the hollow-type coordination complexes, three structures were found (adsorption energies from 5.4 to 9.2 kcal/mol per single H atom). The HCP-type structures (H1, H5) are characterized by the adsorption energies 6.2 and 9.2 kcal/mol, respectively, whereas the adsorption energy of the FCC structure (H2) is 5.4 kcal/mol. In contrast, in our calculations, the adsorption energies at the FCC sites of Pt_{24} are higher (9.1−11.4 kcal/mol) than the energies on the HCP sites (7.8 kcal/mol, which is in the range of the HCP values of ref 34).

The H adsorption on Pt(111), Pt(100), and the edges between them has been studied with the periodic RPBE/PW calculations.[35] In the case of adsorption on Pt(100), the bridge-like adsorption complex was most favorable with a binding energy of about 10.4 kcal/mol, in satisfactory agreement with our estimates for the $\beta\beta$ complex (8.94 kcal/mol). However, in the case of Pt(111) adsorption, the on-top and three-coordinated structures were less favorable (about 8.5 kcal/mol). This value is close to our averaged estimate 8.9 kcal/mol; however, the on-top ε complex is much less favorable in our results. From Figure 5 of ref 35, it is also possible to derive the binding energy for the $L_{\beta\beta}$ complex (about 4.5 kcal/mol). Although this value is obviously influenced by the lateral interactions among other H atoms adsorbed on the surface, it is rather close to our estimate of 5.7 kcal/mol.

In the study,[31] the structure, energy, vibrational frequencies, and thermodynamic parameters of the 55 atom cubooctahedral Pt NP of 1 nm in size with various numbers of adsorbed H atoms was modeled using the periodic cluster RPBE/PW calculations. For the single adsorbed H atom, the bridge-like complexes on the Pt(100) facet and on the edge between Pt(100) and Pt(111) facets (most close in their structure to our $\beta\beta$ complex) have an adsorption energy of 14.0 and 10.9 kcal/mol, respectively. This is higher than our value of 8.9 kcal/mol. The second most favorable structure was the on-top complex on the Pt(100) facet (13.3 kcal/mol) which is not located in our calculations. It should also be noted that the located three-coordinated complex on Pt(111) is the least favorable among all the single-atomic H complexes (3.4 kcal/mol).

Thus, the results obtained in the present study demonstrate the remarkable distinction between the periodic and molecular cluster calculations in the stability of the on-top complexes. This raises the question about the nature of such a distinction. First, the on-top structures of both molecular and atomic hydrogen are much less favorable in our results. In our opinion, this is the consequence of the artificial stabilization of such structures appearing due to the interaction with the ghost atoms of periodically distributed slabs. We found only metastable structures of such complexes, only on the ε

DOI: 10.1021/acs.jpcc.6b04555
J. Phys. Chem. C 2016, 120, 18570−18587

atoms, not on the vertices of the cluster, with relatively low coordination energies for these structures. All structures are easily rearranged to more favorable bridge-like and 2-fold coordinated complexes. We conclude that the on-top coordination on the isolated Pt clusters or NPs are unfavorable. They are also quite unfavorable from the point of view of the molecular hydrogen activation.

The hydrogen diffusion barriers from FCC to HCP sites were estimated in several studies, both experimental[22,27] and theoretical.[24,32,33] In the experimental studies, the barrier heights were estimated as 1.6 kcal/mol in ref 22 by the quasi-elastic He scattering (QHAS) experiments and as 4.4 kcal/mol in ref 27 using the linear optical diffraction (LOD) technique. In theoretical studies,[24,32,33] the estimated activation barriers were in ranges of 1.4−1.8 kcal/mol, in agreement with the QHAS data. However, the results obtained in our study are somewhat closer to the LOD data.[27] Three FCC → HCP barriers ($\gamma\gamma\varepsilon \rightarrow \gamma\delta\varepsilon$, $\beta\delta\varepsilon \rightarrow \gamma\delta\varepsilon$, $\beta\delta\varepsilon \rightarrow \beta\beta\varepsilon$) are of 4.6, 4.1, and 2.5 kcal/mol. At the same time, the corresponding barriers for the back reaction HCP → FCC are 1.0, 2.8, and 1.2 kcal/mol, respectively. Probably, the QHAS and LOD experiments excite the different modes of the hydrogen diffusion transfer, resulting in the different estimates of the barrier heights.

The activation energy of the H and D surface diffusion on Pt(111) experimentally determined with the quasielastic helium atom scattering[22] as 1.6 kcal/mol is remarkably lower than our estimates of 2.5−4.6 kcal/mol for the migration between the adsorption sites on the (111) facet of Pt_{24}. Probably, this disagreement is due to the effect of quantum tunneling which takes place in the case of light H atoms moving on the surface. The effect of such excitations was estimated in ref 24 to be 0.71 kcal/mol on the basis of HREELS spectra and comparison with the calculated vibrational bands of the adsorbed H atoms. It was found that the low-energy vibrational excitations corresponding to the observed HREELS peak at 31 meV (0.71 kcal/mol) have a localized character (they are lower than the estimated classical activation barrier). At higher excitations (registered peak at 60 meV, 1.4 kcal/mol), the H movements are mostly delocalized, although the energy is lower than the barrier heights. This supports the suggestion about the quantum tunneling of H atoms on the Pt surface. If so, our estimations can be considered as an upper border for the diffusion barrier in a classical approximation staying in agreement with the experimental data. On the basis of the PES profiles and vibrational frequencies obtained in the present study, it is possible to estimate the tunneling probabilities for such a process.

There exist also theoretical works considering the energies and barriers of the dissociative adsorption (or reverse associative desorption) of hydrogen on the Pt clusters and NPs of various shapes and sizes.

In the study,[28] the clusters Pt_nH and Pt_nH_2 (n = 1−5) were considered at the BPW91/LANL2DZ/6-311++G(d,p) theory level. Binding energies of H atoms at Pt_5 were estimated as 64−66 kcal/mol, the adsorption energy of H_2 was 8.6−10.0 kcal/mol (relative to the free H_2 molecule), and the energy of the dissociated H_2 molecule was 2.2−9.1 kcal/mol (relative to free H_2). Because the structures located in their work are mostly bridge-like, the adsorption energies are in good agreement with our estimates of the H binding energies at the bridge-type complexes (5.2−8.9 kcal/mol).

In the study,[30] H_2 desorption from $Pt_{13}H_{24}$ (completely covered surface) was modeled with AIMD in the quasi-periodic cluster calculations using the PBE functional in the plane wave basis. They estimated the activation energy of the H_2 desorption from the $Pt_{13}H_{24}$ cluster as 12.2 kcal/mol, and the corresponding energy of dissociative adsorption of H_2 is about 3.3 kcal/mol per single H atom relative to the H_2 and $Pt_{13}H_{22}$ reactants (estimated from Figure 7 of ref 30). The first value is close to our results for bridge- and three-coordinated Pt_{24}−H complexes, and the second one is 2−3 times lower than the corresponding barrier estimated as the desorption energy from the 2- or 3-fold coordinated complexes.

The estimates of the activation barriers for the subsurface diffusion (5.4 and 8.2 kcal/mol) are comparable for the results obtained in ref 76 on the spillover of H from the Pt_4 clusters to the oxygen-doped graphite support covered by epoxide groups (see also other studies of the spillover from Pt clusters to graphite, grapheme, and boron nitride supports where much higher barriers were found[77−79]). It was established that the activation energy of such a spillover to the oxygen containing carbon support is about 9.2 kcal/mol.

Thus, the upper border of the activation energy for the subsurface diffusion of H is comparable with the activation energies of typical reactions occurring at the Pt surface including the rate limiting step of H atom migration from Pt clusters to the oxide supports. On the basis of the results obtained, we conclude that the Pt_{24} subsurface diffusion is not a limiting step of the spillover process occurring on the Pt NPs covered by the surface ligands tackling the surface hydrogen migration.

CONCLUSIONS

1. The subnanosized cluster Pt_{24} was applied as a representative model of the small-size or size-selected Pt-NPs, e.g., formed in the zeolite pores. The studied cluster structure is more favorable in energy than the global minimum of Pt_{24} described earlier. The most low-lying spin states of the cluster are M = 3, 5, 7, 9 among which the quintet state is the ground one and the energy difference between the low-lying states is under 1 kcal/mol. Symmetry and presence of different microfacets of the cluster surface is convenient in describing the molecular and dissociative adsorption of molecular hydrogen, the H_2 dissociation in an adsorbed state, the coordination, surface and subsurface diffusion of H atoms on various sites on the NP surface at low-coverage modes. This also opens the possibility to explore the full map of adsorption sites and pathways of surface processes taking place at the similar Pt NPs.
2. Six coordination modes were found for the molecular hydrogen adsorption of Pt_{24} including on-top adsorption, lateral coordination on a single Pt atom, and two kinds of bridge-like adsorption complexes. The coordination of molecular hydrogen on a Pt_{24} cluster is characterized by average coordination energies of 4.57 kcal/mol. The most favorable structures are the bridge-like structures, whereas the on-top coordination is the least favorable.
3. The energies of H atom coordination are significantly different on different surface sites. The most favorable coordination takes place at the three-coordinated (hollow) site corresponding to the FCC site of an ideal Pt(111) surface. The on-top coordination is quite unfavorable, in sharp contradiction with the results of many periodic calculations.

DOI: 10.1021/acs.jpcc.6b04555
J. Phys. Chem. C 2016, 120, 18570−18587

4. The surface diffusion inside the Pt_{24} cluster is characterized by the activation barriers estimated as 4.4 and 8.2 kcal/mol. Thus, the upper limit of the activation energy for the spillover process occurring through the subsurface diffusion of H is not high and comparable with the activation energies of many reactions occurring at the Pt surface.
5. The IR and Raman spectra of the adsorbed H atoms obtained in the present work can be in principle used for the experimental distinguishing between different adsorption modes.

■ ASSOCIATED CONTENT

Supporting Information

The Supporting Information is available free of charge on the ACS Publications website at DOI: 10.1021/acs.jpcc.6b04555.

Optimized Cartesian coordinates, total energies, and calculated thermodynamic parameters for source cluster structures in several spin states and their coordination complexes with molecular and atomic hydrogen (PDF)

■ AUTHOR INFORMATION

Corresponding Author

*E-mail: ignatov@ichem.unn.ru. Phone/Fax: +7 (831) 462 32 20.

Notes

The authors declare no competing financial interest.

■ ACKNOWLEDGMENTS

This work was supported by the Russian Foundation for Basic Research (Project No. 14-03-00585). O.B.G. and A.I.O. are thankful to DAAD and the International Office of the University of Bremen.

■ REFERENCES

(1) *Hydrogen as a Future Energy Carrier*; Züttel, A., Borgschulte, A., Schlapbach, L., Eds.; Wiley-VCH Verlag GmbH & Co. KGaA: Weinheim, Germany, 2008; p 427.

(2) Rifkin, J. *The Hydrogen Economy: the Creation of the Worldwide Energy Web and the Redistribution of Power on Earth*; J.P. Tarcher Inc. Penguin Group: New York, 2003; p 304.

(3) Schlapbach, L.; Züttel, A. Hydrogen-storage Materials for Mobile Applications. *Nature* **2001**, *414*, 353−358.

(4) Prabhu, S.; Frank, S. Hydrogen Sensing and Detection. In *Hydrogen Fuel. Production, Transport, and Storage*; Gupta, R. B., Ed.; CRC Press, Taylor and Francis Group, LLC.: New York, 2008; pp 495−534.

(5) Morsbach, E.; Kunz, S.; Bäumer, M. Novel Nanoparticle Catalysts for Catalytic Gas Sensing. *Catal. Sci. Technol.* **2016**, *6*, 339−348.

(6) Brauns, E.; Morsbach, E.; Kunz, S.; Bäumer, M.; Lang, W. Temperature Modulation of a Catalytic Gas Sensor. *Sensors* **2014**, *14*, 20372−20381.

(7) Bockris, J. O. M.; Khan, S. U. M. *Surface Electrochemistry. A Molecular Level Approach*; Springer US, Plenum Press: New York, 1993; p 976.

(8) Skulason, E.; Karlberg, G. S.; Rossmeisl, J.; Bligaard, T.; Greeley, J.; Jonsson, H.; Norskov, J. K. Density Functional Theory Calculations for the Hydrogen Evolution Reaction in an Electrochemical Double Layer on the Pt(111) Electrode. *Phys. Chem. Chem. Phys.* **2007**, *9*, 3241−3250.

(9) Heitbaum, M.; Glorius, F.; Escher, I. Asymmetric Heterogeneous Catalysis. *Angew. Chem., Int. Ed.* **2006**, *45*, 4732−4762.

(10) Yan, J.; Ouyang, R.; Jensen, P. S.; Ascic, E.; Tanner, D.; Mao, B.; Zhang, J.; Tang, C.; Hush, N. S.; Ulstrup, J.; Reimers, J. R. Controlling the Stereochemistry and Regularity of Butanethiol Self-Assembled Monolayers on Au(111). *J. Am. Chem. Soc.* **2014**, *136*, 17087−17094.

(11) Grirrane, A.; Corma, A.; Garcia, H. Stereoselective Single (Copper) or Double (Platinum) Boronation of Alkynes Catalyzed by Magnesia-Supported Copper Oxide or Platinum Nanoparticles. *Chem. - Eur. J.* **2011**, *17*, 2467−2478.

(12) Yoon, M.; Srirambalaji, R.; Kim, K. Homochiral Metal−Organic Frameworks for Asymmetric Heterogeneous Catalysis. *Chem. Rev.* **2012**, *112*, 1196−1231.

(13) Schrader, I.; Neumann, S.; Himstedt, R.; Zana, A.; Warneke, J.; Kunz, S. The Effect of Particle Size and Ligand Configuration on the Asymmetric Catalytic Properties of Proline-functionalized Pt-nanoparticles. *Chem. Commun.* **2015**, *51*, 16221−16224.

(14) Schrader, I.; Warneke, J.; Backenköhler, J.; Kunz, S. Functionalization of Platinum Nanoparticles with l-Proline: Simultaneous Enhancements of Catalytic Activity and Selectivity. *J. Am. Chem. Soc.* **2015**, *137*, 905−912.

(15) Miyazaki, A.; Balint, I. Synthesis of Morphologically Controlled Pt Nanoparticles and Their Application in Catalytic Reactions. In *Metal Nanoclusters in Catalysis and Materials Science: The Issue of Size Control*; Corain, B., Schmid, G., Toshima, N., Eds.; Elsevier: Amsterdam, The Netherlands, 2008; Chapter 16, pp 301−305.

(16) Veith, G. M.; Lupini, A. R.; Dudney, N. J. Magnetron Sputtering to Prepare Supported Metal Catalysts. In *Metal Nanoclusters in Catalysis and Materials Science: The Issue of Size Control*; Corain, B., Schmid, G., Toshima, N., Eds.; Elsevier: Amsterdam, The Netherlands, 2008; Chapter 21, pp 347−353.

(17) Roduner, E.; Jensen, C. Magnetic Properties and the Superatom Character of 13-Atom Platinum Nanoclusters. *Magnetochemistry* **2015**, *1*, 28−44.

(18) Christmann, K.; Ertl, G.; Pignet, T. Adsorption of Hydrogen on a Pt(111) Surface. *Surf. Sci.* **1976**, *54*, 365−392.

(19) Poelsema, B.; Mechtersheimer, G.; Comsa, G. The Interaction of Hydrogen with Platinum(s)−9(111) × (111) Studied with Helium Beam Diffraction. *Surf. Sci.* **1981**, *111*, 519−544.

(20) Pennemann, B.; Oster, K.; Wandelt, K. Activated Hydrogen Adsorption on the Pt(100) 1 × 1 Surface. *Surf. Sci.* **1991**, *251-252*, 877−881.

(21) Klötzer, B.; Bechtold, E. Hydrogen Adsorption and the Transformation of the Pt(100) Surface Structure. *Surf. Sci.* **1993**, *295*, 374−384.

(22) Graham, A. P.; Menzel, A.; Toennies, J. P. Quasielastic Helium Atom Scattering Measurements of Microscopic Diffusional Dynamics of H and D on the Pt(111) Surface. *J. Chem. Phys.* **1999**, *111*, 1676−1685.

(23) Poelsema, B.; Lenz, K.; Comsa, G. The Dissociative Adsorption of Hydrogen on Defect-'Free' Pt(111). *J. Phys.: Condens. Matter* **2010**, *22*, 304006-1−304006-10.

(24) Bădescu, Ş. C.; Salo, P.; Ala-Nissila, T.; Ying, S. C.; Jacobi, K.; Wang, Y.; Bedürftig, K.; Ertl, G. Energetics and Vibrational States for Hydrogen on Pt(111). *Phys. Rev. Lett.* **2002**, *88*, 136101-1−136101-4.

(25) Gudmundsdottir, S.; Skulason, E.; Weststrate, K.-J.; Juurlink, L.; Jonsson, H. Hydrogen Adsorption and Desorption at the Pt(110)-(1 × 2) Surface: Experimental and Theoretical Study. *Phys. Chem. Chem. Phys.* **2013**, *15*, 6323−6332.

(26) Bond, G. C. *Metal-Catalysed Reactions of Hydrocarbons*; Springer US: Boston, MA, 2005; p 655.

(27) Zheng, C. Z.; Yeung, C. K.; Loy, M. M. T.; Xiao, X. Quantum Diffusion of H on Pt(111): Step Effects. *Phys. Rev. Lett.* **2006**, *97*, 166101-1−166101-4.

(28) Sebetci, A. A Density Functional Study of Bare and Hydrogenated Platinum Clusters. *Chem. Phys.* **2006**, *331*, 9−18.

(29) Sebetci, A. New Minima for the Pt8 Cluster. *Comput. Mater. Sci.* **2013**, *78*, 9−11.

(30) Meng, Q.; May, P. S.; Berry, M. T.; Kilin, D. Sequential Hydrogen Dissociation from a Charged $Pt_{13}H_{24}$ Cluster Modeled by Ab Initio Molecular Dynamics. *Int. J. Quantum Chem.* **2012**, *112*, 3896−3903.

DOI: 10.1021/acs.jpcc.6b04555
J. Phys. Chem. C 2016, 120, 18570−18587

(31) Tan, T. L.; Wang, L.-L.; Zhang, J.; Johnson, D. D.; Bai, K. Platinum Nanoparticle During Electrochemical Hydrogen Evolution: Adsorbate Distribution, Active Reaction Species, and Size Effect. *ACS Catal.* **2015**, *5*, 2376−2383.
(32) Källén, G.; Wahnström, G. Quantum treatment of H Adsorbed on a Pt(111) Surface. *Phys. Rev. B: Condens. Matter Mater. Phys.* **2001**, *65*, 033406-1−033406-4.
(33) Kristinsdóttir, L.; Skúlason, E. A systematic DFT Study of Hydrogen Diffusion on Transition Metal Surfaces. *Surf. Sci.* **2012**, *606*, 1400−1404.
(34) Hu, M.; Linder, D. P.; Buongiorno Nardelli, M.; Striolo, A. Hydrogen Adsorption on Platinum−Gold Bimetallic Nanoparticles: A Density Functional Theory Study. *J. Phys. Chem. C* **2013**, *117*, 15050−15060.
(35) Skúlason, E.; Faraj, A.; Kristinsdóttir, L.; Hussain, J.; Garden, A.; Jónsson, H. Catalytic Activity of Pt Nano-Particles for H_2 Formation. *Top. Catal.* **2014**, *57*, 273−281.
(36) Ford, D. C.; Xu, Y.; Mavrikakis, M. Atomic and Molecular Adsorption on Pt(1 1 1). *Surf. Sci.* **2005**, *587*, 159−174.
(37) Zyubin, A. S.; Zyubina, T. S.; Dobrovol'skii, Y. A.; Volokhov, V. M. Behavior of Molecular Hydrogen on the Platinum Crystal Surface: Quantum-chemical Modeling. *Russ. J. Inorg. Chem.* **2012**, *57*, 1460−1469.
(38) Yang, S. H.; Drabold, D. A.; Adams, J. B.; Ordejón, P.; Glassford, K. Density Functional Studies of Small Platinum Clusters. *J. Phys.: Condens. Matter* **1997**, *9*, L39−L45.
(39) Aprà, E.; Fortunelli, A. Density-Functional Calculations on Platinum Nanoclusters: Pt_{13}, Pt_{38}, and Pt_{55}. *J. Phys. Chem. A* **2003**, *107*, 2934−2942.
(40) Tian, W. Q.; Ge, M.; Sahu, B. R.; Wang, D.; Yamada, T.; Mashiko, S. Geometrical and Electronic Structure of the Pt_7 Cluster: A Density Functional Study. *J. Phys. Chem. A* **2004**, *108*, 3806−3812.
(41) Xiao, L.; Wang, L. Structures of Platinum Clusters: Planar or Spherical?†. *J. Phys. Chem. A* **2004**, *108*, 8605−8614.
(42) Yuan, H. K.; Chen, H.; Kuang, A. L.; Wu, B. Spin−orbit Effect and Magnetic Anisotropy in Pt clusters. *J. Magn. Magn. Mater.* **2013**, *331*, 7−16.
(43) Li, L.; Larsen, A. H.; Romero, N. A.; Morozov, V. A.; Glinsvad, C.; Abild-Pedersen, F.; Greeley, J.; Jacobsen, K. W.; Nørskov, J. K. Investigation of Catalytic Finite-Size-Effects of Platinum Metal Clusters. *J. Phys. Chem. Lett.* **2013**, *4*, 222−226.
(44) Huda, M. N.; Kleinman, L. Hydrogen Adsorption and Dissociation on Small Platinum Clusters: An Electronic Structure Density Functional Study. *Phys. Rev. B: Condens. Matter Mater. Phys.* **2006**, *74*, 195407-1−195407-7.
(45) Zhou, C.; Wu, J.; Nie, A.; Forrey, R. C.; Tachibana, A.; Cheng, H. On the Sequential Hydrogen Dissociative Chemisorption on Small Platinum Clusters: A Density Functional Theory Study. *J. Phys. Chem. C* **2007**, *111*, 12773−12778.
(46) Nieminen, V.; Honkala, K.; Taskinen, A.; Murzin, D. Y. Intrinsic Metal Size Effect on Adsorption of Organic Molecules on Platinum. *J. Phys. Chem. C* **2008**, *112*, 6822−6831.
(47) Busygin, I.; Taskinen, A.; Nieminen, V.; Toukoniitty, E.; Stillger, T.; Leino, R.; Murzin, D. Y. Experimental and Theoretical Analysis of Asymmetric Induction in Heterogeneous Catalysis: Diastereoselective Hydrogenation of Chiral α-Hydroxyketones over Pt Catalyst. *J. Am. Chem. Soc.* **2009**, *131*, 4449−4462.
(48) Kozlov, S. M.; Aleksandrov, H. A.; Neyman, K. M. Adsorbed and Subsurface Absorbed Hydrogen Atoms on Bare and MgO(100)-Supported Pd and Pt Nanoparticles. *J. Phys. Chem. C* **2014**, *118*, 15242−15250.
(49) Kozlov, S. M.; Aleksandrov, H. A.; Neyman, K. M. Energetic Stability of Absorbed H in Pd and Pt Nanoparticles in a More Realistic Environment. *J. Phys. Chem. C* **2015**, *119*, 5180−5186.
(50) de Graaf, J.; van Dillen, A. J.; de Jong, K. P.; Koningsberger, D. C. Preparation of Highly Dispersed Pt Particles in Zeolite Y with a Narrow Particle Size Distribution: Characterization by Hydrogen Chemisorption, TEM, EXAFS Spectroscopy, and Particle Modeling. *J. Catal.* **2001**, *203*, 307−321.
(51) Altmann, L.; Kunz, S.; Bäumer, M. Influence of Organic Amino and Thiol Ligands on the Geometric and Electronic Surface Properties of Colloidally Prepared Platinum Nanoparticles. *J. Phys. Chem. C* **2014**, *118*, 8925−8932.
(52) Alonso-Vante, N. Platinum and Non-Platinum Nanomaterials for the Molecular Oxygen Reduction Reaction. *ChemPhysChem* **2010**, *11*, 2732−2744.
(53) Holade, Y.; Sahin, N.; Servat, K.; Napporn, T.; Kokoh, K. Recent Advances in Carbon Supported Metal Nanoparticles Preparation for Oxygen Reduction Reaction in Low Temperature Fuel Cells. *Catalysts* **2015**, *5*, 310−348.
(54) Magalhães, M. M.; Colmati, F. Carbon-supported PtSnCu, PtCu and PtSn electrocatalysts for ethanol oxidation in acid media. *J. Braz. Chem. Soc.* **2014**, *25*, 1317−1325.
(55) Ross, R. B.; Powers, J. M.; Atashroo, T.; Ermler, W. C.; LaJohn, L. A.; Christiansen, P. A. Abinitio Relativistic Effective Potentials With Spin−Orbit Operators. IV. Cs through Rn. *J. Chem. Phys.* **1990**, *93*, 6654−6670.
(56) Frisch, M. J.; Trucks, G. W.; Schlegel, H. B.; Scuseria, G. E.; Robb, M. A.; Cheeseman, J. R.; Montgomery, J. A., Jr.; Vreven, T.; Kudin, K. N.; Burant, J. C.; et al. *Gaussian 03*, version D.02; Gaussian, Inc.: Wallingford, CT, 2007.
(57) Ignatov, S. K. *MOLTRAN*, version 2.7; University of Nizhny Novgorod: Nizhny Novgorod, Russia, 2009. URL: http://www.unn.ru/chem/moltran/ (accessed March 27, 2016).
(58) Ignatov, S. K. *Moltran − a program for the thermodynamic calculations assessing the internal rotations in non-rigid molecules, Book of Theses*, XX International Conference on Chemical Thermodynamic in Russia RCCT-2015, University of Nizhny Novgorod, Nizhni Novgorod, Russia, May 22−26, 2015.
(59) Zhurko, G. *ChemCraft*, version 1.7 (build 365). URL: http://www.chemcraftprog.com (accessed March 27, 2016).
(60) Doye, J. P. K.; Wales, D. J. Global Minima for Transition Metal Clusters Described by Sutton-Chen potentials. *New J. Chem.* **1998**, *22*, 733−744.
(61) Sutton, A. P.; Chen, J. Long-range Finnis−Sinclair Potentials. *Philos. Mag. Lett.* **1990**, *61*, 139−146.
(62) Sebetci, A.; Güvenç, Z. B. Global Minima for Free Pt_N Clusters (N = 22−56): a Comparison between the Searches with a Molecular Dynamics Approach and a Basin-hopping Algorithm. *Eur. Phys. J. D* **2004**, *30*, 71−79.
(63) Sebetci, A.; Güvenç, Z. B. Global Minima of Al_N, Au_N and Pt_N, $N \leq 80$, Clusters Described by the Voter−Chen Version of Embedded-atom Potentials, Modell. *Modell. Simul. Mater. Sci. Eng.* **2005**, *13*, 683−698.
(64) Nie, A.; Wu, J.; Zhou, C.; Yao, S.; Luo, C.; Forrey, R. C.; Cheng, H. Structural Evolution of Subnano Platinum Clusters. *Int. J. Quantum Chem.* **2007**, *107*, 219−224.
(65) Gupta, R. P. Lattice Relaxation at a Metal Surface. *Phys. Rev. B: Condens. Matter Mater. Phys.* **1981**, *23*, 6265−6270.
(66) Zhang, J.; Dolg, M. ABCluster: The Artificial Bee Colony Algorithm for Cluster Global Optimization. *Phys. Chem. Chem. Phys.* **2015**, *17*, 24173−24181.
(67) Davidson, E. R.; Clark, A. E. Spin Polarization and Annihilation for Radicals and diradicals. *Int. J. Quantum Chem.* **2005**, *103*, 1−9.
(68) Plakhutin, B. N.; Gorelik, E. V.; Breslavskaya, N. N.; Milov, M. A.; Fokeyev, A. A.; Novikov, A. V.; Prokhorov, T. E.; Polygalova, N. E.; Dolin, S. P.; Trakhtenberg, L. I. Anomalous Values of $\langle \hat{S}^2 \rangle$ Before and After Annihilation of the First Spin Contaminant in UHF Wave Function. *J. Struct. Chem.* **2005**, *46*, 195−203.
(69) Vannice, M. A.; Hasselbring, L. C.; Sen, B. Direct Measurements of Heats of Adsorption on Platinum Catalysts. *J. Catal.* **1985**, *95*, 57−70.
(70) Sen, B.; Chou, P.; Vannice, M. A. Direct Measurements of Heats of Adsorption on Platinum Catalysts. *J. Catal.* **1986**, *101*, 517−521.
(71) Richter, L. J.; Ho, W. Vibrational Spectroscopy of H on Pt(111): Evidence for Universally Soft Parallel Modes. *Phys. Rev. B: Condens. Matter Mater. Phys.* **1987**, *36*, 9797−9800.

DOI: 10.1021/acs.jpcc.6b04555
J. Phys. Chem. C 2016, 120, 18570−18587

(72) Mate, C. M.; Bent, B. E.; Somorjai, G. A. Vibrational spectroscopy of hydrogen adsorbed on metal surfaces. In *Hydrogen Effects in Catalysis: Fundamentals and Practical Applications*; Paan, Z., Menon, P. G., Eds.; Marcel Dekker, Inc.: New York, Basel, 1988; Chapter 2, pp 57−85.
(73) Spiewak, B. E.; Dumesic, J. A. Microcalorimetric Measurements of Differential Heats of Adsorption on Reactive Catalyst Surfaces. *Thermochim. Acta* **1997**, *290*, 43−53.
(74) Sharma, S. B.; Miller, M. T.; Dumesic, J. A. Microcalorimetric Study of Silica- and Zeolite-Supported Platinum Catalysts. *J. Catal.* **1994**, *148*, 198−204.
(75) Spiewak, B. E.; Cortright, R. D.; Dumesic, J. A. Microcalorimetric Studies of H_2, C_2H_4, and C_2H_2 Adsorption on Pt Powder. *J. Catal.* **1998**, *176*, 405−414.
(76) Psofogiannakis, G. M.; Froudakis, G. E. DFT Study of Hydrogen Storage by Spillover on Graphite with Oxygen Surface Groups. *J. Am. Chem. Soc.* **2009**, *131*, 15133−15135.
(77) Psofogiannakis, G. M.; Froudakis, G. E. DFT Study of the Hydrogen Spillover Mechanism on Pt-Doped Graphite. *J. Phys. Chem. C* **2009**, *113*, 14908−14915.
(78) Wu, H.-Y.; Fan, X.; Kuo, J.-L.; Deng, W.-Q. DFT Study of Hydrogen Storage by Spillover on Graphene with Boron Substitution. *J. Phys. Chem. C* **2011**, *115*, 9241−9249.
(79) Wu, X.; Yang, J. L.; Zeng, X. C. Adsorption of Hydrogen Molecules on the Platinum-Doped Boron Nitride Nanotubes. *J. Chem. Phys.* **2006**, *125*, 044704-1−044704-6.

DOI: 10.1021/acs.jpcc.6b04555
J. Phys. Chem. C 2016, 120, 18570−18587